ELSEVIER

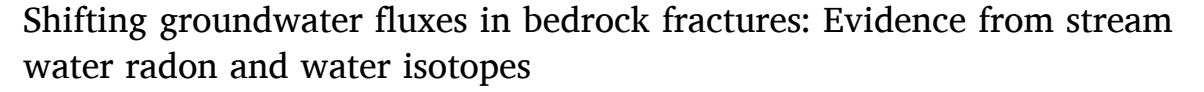
Contents lists available at ScienceDirect

Journal of Hydrology

journal homepage: www.elsevier.com/locate/jhydrol



Research papers



Keira Johnson^{a,*}, John N. Christensen^b, W. Payton Gardner^c, Matthias Sprenger^b, Li Li ^d, Kenneth H. Williams^{b,e}, Rosemary W.H. Carroll^f, Nicholas Thiros^b, Wendy Brown^g, Curtis Beutler^g, Alexander Newman^g, Pamela L. Sullivan^{a,*}

- ^a College of Earth, Ocean, and Atmospheric Sciences, Oregon State University, USA
- ^b Lawrence Berkeley National Laboratory, Berkeley, CA, USA
- ^c Dept. of Geosciences, University of Montana, MT, USA
- ^d Department of Civil and Environmental Engineering, Penn State University, USA
- e Rocky Mountain Biological Laboratory, Gothic, CO, USA
- f Desert Research Institute, Reno, NV, USA
- ^g The Rocky Mountain Biological Laboratory, Gothic, CO USA

ARTICLE INFO

Keywords: Groundwater surface water interactions Tracer hydrology Groundwater modeling Groundwater discharge Montane catchment

ABSTRACT

Geologic features (e.g., fractures and alluvial fans) can play an important role in the locations and volumes of groundwater discharge and degree of groundwater-surface water (GW-SW) interactions. However, the role of these features in controlling GW-SW dynamics and streamflow generation processes are not well constrained. GW-SW interactions and streamflow generation processes are further complicated by variability in precipitation inputs from summer and fall monsoon rains, as well as declines in snowpack and changing melt dynamics driven by warming temperatures. Using high spatial and temporal resolution radon and water stable isotope sampling and a 1D groundwater flux model, we evaluated how groundwater contributions and GW-SW interactions varied along a stream reach impacted by fractures (fractured-zone) and downstream of the fractured hillslope (nonfractured zone) in Coal Creek, a Colorado River headwater stream affected by summer monsoons. During early summer, groundwater contributions from the fractured zone were high, but declined throughout the summer. Groundwater contributions from the non-fractured zone were constant throughout the summer and became proportionally more important later in the summer. We hypothesize that groundwater in the non-fractured zone is dominantly sourced from a high-storage alluvial fan at the base of a tributary that is connected to Coal Creek throughout the summer and provides consistent groundwater influx. Water isotope data revealed that Coal Creek responds quickly to incoming precipitation early in the summer, and summer precipitation becomes more important for streamflow generation later in the summer. We quantified the change in catchment dynamic storage and found it negatively related to stream water isotope values, and positively related to modeled groundwater discharge and the ratio of fractured zone to non-fractured zone groundwater. We interpret these relationships as declining hydrologic connectivity throughout the summer leading to late summer streamflow supported predominantly by shallow flow paths, with variable response to drying from geologic features based on their storage. As groundwater becomes more important for sustaining summer flows, quantifying local geologic controls on groundwater inputs and their response to variable moisture conditions may become critical for accurate predictions of streamflow.

1. Introduction

Streamflow derived from montane environments is important for downstream communities and ecosystem services but is vulnerable due to decreasing snowpack resulting from climate change (Viviroli et al., 2007; Mote et al., 2018; Viviroli et al., 2020). Earlier peak flows, smaller snowpacks, and higher evapotranspiration rates are predicted to decrease summer flows (Stewart et al., 2005; Bayay et al., 2009; Ficklin

E-mail addresses: johnkeir@oregonstate.edu (K. Johnson), pamela.sullivan@oregonstate.edu (P.L. Sullivan).

https://doi.org/10.1016/j.jhydrol.2024.131202

^{*} Corresponding authors.

et al., 2013; Azmat et al., 2017) leading to an increased reliance on groundwater (Kapnick and Hall, 2012; Somers et al., 2019). The relationship between groundwater and surface water (termed GW-SW interactions) is dominantly influenced by precipitation regime, vegetation, and geologic setting (Banks et al., 2011; Andermann et al., 2012; Safeeq et al., 2013; Carroll et al., 2018; Brooks et al., 2021). Especially of interest is summer precipitation (e.g., monsoon rains) which can contribute large amounts of water in the summer months (Sheppard et al., 2002) and have the potential to buffer summer flows during low snowpack years (Carroll et al., 2020). Few studies have documented the impacts of monsoon rains on groundwater contribution in montane, snow dominated watersheds due to the remote nature of these catchments (Somers and McKenzie, 2020). Our understanding of GW-SW interactions can be enhanced with an improved quantification of the impacts of monsoon rains on groundwater contributions to summer flow, which sustains streamflow across the mountainous West.

GW-SW interactions are often difficult to quantify given the complex controls that geology exerts on spatial and temporal patterns of groundwater discharge (McClymont et al., 2012; Floriancic et al., 2018). Geologic features can play an important role in the locations and volume of groundwater discharge (Banks et al., 2009; Andermann et al., 2012). For example, in hard rock systems, groundwater predominantly flows through fractures due to their relatively higher permeability as compared to the surrounding matrix (Oxtobee and Novakowski, 2003). Groundwater in fractures can respond quickly to precipitation inputs (Flerchinger et al., 1993; Salve et al., 2012; Webb et al., 2017), rapidly recharging aquifers (Wittenberg et al., 2019) and discharging to streams (McDonnell, 1990). Alluvial deposits can also form in hard rock systems from long periods of sediment transport and deposition or glacial erosion. These deposits behave nearly opposite of fractured bedrock; they are characterized by high storage and have the potential to contribute large amounts of groundwater to summer stream flow over extended periods of time (Liu et al., 2004; Gordon et al., 2015; Käser and Hunkeler, 2016).

Hydrologic connectivity determines how different subsurface storage reservoirs contribute to surface water, and changes in hydrologic connectivity can be driven by changes in moisture conditions (Covino, 2017). Dynamic storage can be used as a proxy for hydrologic connectivity, where periods of higher dynamic storage indicate higher hydrologic connectivity (McIntosh et al., 2017; Dwivedi et al., 2019). Dynamic storage is part of overall catchment storage and defined as the variation in storage between wet and dry periods (Spence, 2007; Kirchner, 2009; Sayama et al., 2011; Dwivedi et al., 2019). Estimations of dynamic storage have been leveraged to estimate subsurface storage (Sayama et al., 2011) and perform hydrograph separation (Dwivedi et al., 2019), and can be combined with other tracers to gain insights into flow path length and origin at the catchment scale. In montane environments, periods of high hydrologic connectivity typically occur during snowmelt, and recede throughout the summer (Jencso et al., 2010). However, in monsoon-impacted catchments, we expect that significant rainfall in the summer and fall months may temporarily increase hydrologic connectivity facilitating changes in GW-SW interactions. Additionally, we expect that the difference in storage capacity among geologic features in a catchment will cause them to respond variably to changes in moisture throughout the year, leading to shifts in dominant groundwater contributions throughout the summer (Käser and Hunkeler, 2016; Floriancic et al., 2018; Bush et al., 2023).

It is common to use geochemical and radioisotope tracers to quantify groundwater contribution to streamflow (Liu et al., 2004; Gardner et al., 2011; Gordon et al., 2015; Cowie et al., 2017; Beisner et al., 2018; Carroll et al., 2018). Radon (²²²Rn; half-life 3.8 days) is an effective tracer because of its elevated concentration in groundwater from the continuous decay of uranium in rocks and soils (Webb et al., 2017). Compared to other geochemical tracers, ²²²Rn helps identify locations of high groundwater contribution because it degasses upon interaction with the atmosphere. Thus, areas of high ²²²Rn concentrations indicate

localized groundwater flux into the stream. Radon has been used to assess groundwater contributions across a variety of environments including floodplains (Webb et al., 2017), urban rivers (Schubert et al., 2020), coastal streams (Peterson et al., 2010), mountain streams (Avery et al., 2018), and boreal lakes (Schmidt et al., 2010). Despite the wide range in geomorphic setting, few studies exist that use ²²²Rn to identify groundwater contributions in montane environments (Gleeson et al., 2018). Radon can also be paired with non-degassing geochemical tracers to assess reach- or catchment-scale groundwater contribution (Genereux et al., 1993; Beisner et al., 2018; Gleeson et al., 2018; Liao et al., 2021). Stable water isotopes are a valuable tracer because they are conservative and are commonly used to assess groundwater contribution to montane streams (Fischer et al., 2015; Singh et al., 2016; Segura et al., 2019; Zuecco et al., 2018). Additionally, water isotopes vary with precipitation phase and season allowing for separation of streamflow into seasonal precipitation contributions (Allen et al., 2019a).

Significant advances in montane hydrodynamics could be achieved if the connectivity of geologic features to surface water could be more readily quantified. The aim of this paper is to understand how monsoon rains influence GW-SW interactions in bedrock fractures in a headwater stream of the Colorado River. We use ²²²Rn and stable water isotopes to explore the seasonal variation of groundwater discharge in Coal Creek, a Colorado River headwater stream (Fig. 1a,b). To capture the influence of summer precipitation on groundwater discharge we collected, roughly weekly, synoptic stream ²²²Rn and water isotope samples across a stream reach of Coal Creek influenced by hillslope fractures. We focus on Coal Creek because the geologic setting gives rise to significant fracture networks (Fig. 1c) and because of its potential for high monsoon efficiency (Carroll et al., 2020). Synoptic stream chemistry data were used to constrain a one-dimensional advective-dispersion model to estimate lateral groundwater discharge along the stream length throughout the summer.

2. Methods

2.1. Study site

Coal Creek is a small (53 km²), high-elevation, headwater tributary to the Upper Colorado Basin located on the traditional homelands of the Núu-agha-tv-p (Ute) peoples in the Ruby-Anthracite Range in the central Colorado Rocky Mountains. Coal Creek is located within the larger East River watershed (catchment area of 300 km²), which is a designated Science Focus Area (Hubbard et al., 2018) by the Department of Energy and a watershed observatory within the Critical Zone Collaborative Network (CZCN) supported by the National Science Foundation. As such, the East River, including Coal Creek, hosts a diverse collection of hydro-biogeochemical measurements that provide an ideal setting for examining the controls of groundwater inputs under summer monsoon conditions. The East River and its key tributary drainages are broadly representative of snow-dominated basins in the Rocky Mountains.

Coal Creek ranges in elevation from 2712 to 3668 m. Coal Creek originates near Lake Irwin and enters the Slate River near the town of Crested Butte before joining the East River and eventually the Gunnison River. The watershed is seasonally snow-covered from November through June. The average temperature is 0.9°C and it receives around 670 mm of precipitation each year, about 66 % of which falls as snow (Carroll et al., 2018). The remaining precipitation falls during the summer monsoon season (July through September). Although monsoon rains comprise approximately 25 % of the annual precipitation, they contribute only about 10 % to the summer streamflow because the moisture is lost via evapotranspiration (Carroll et al., 2020; Sprenger et al., 2022). Vegetation in the basin is strongly aspect driven, with north facing aspects dominated by evergreen forest (65 %) and south facing aspects dominated by deciduous (9 %) and herbaceous (20 %) vegetation. High elevation ridges are barren (3 %) (Zhi et al., 2019). Discharge in Coal Creek is dominated by snowmelt, with average peak flow

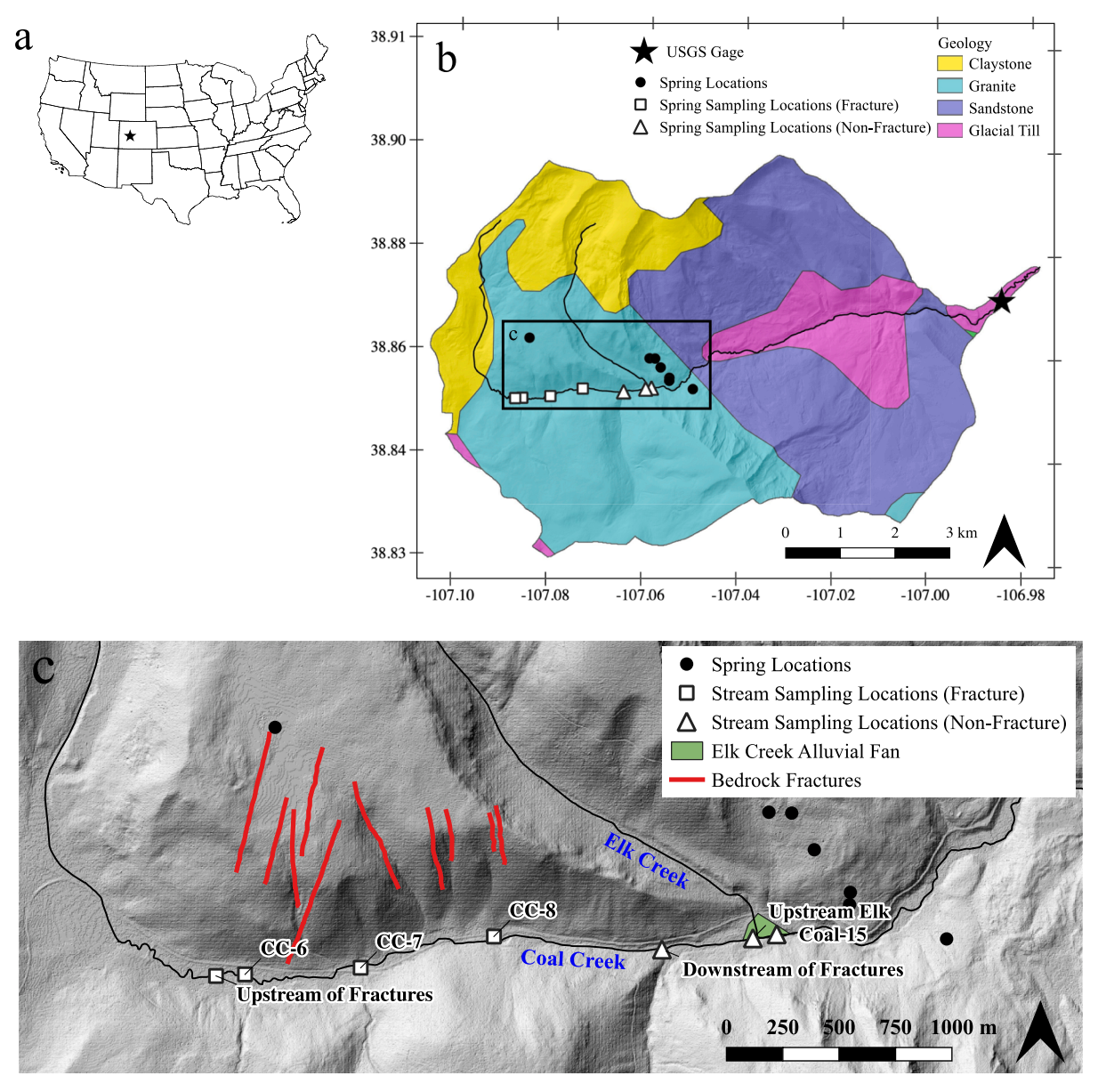


Fig. 1. (a) Location of Coal Creek watershed within the United States. (b) Geologic map of Coal Creek (Horton et al., 2017) watershed showing stream sampling within fracture (white square) and non-fracture (white triangle) zones, spring sampling (black circles) locations, and the Coal Creek USGS gage (black star). (c) Inset of sampling sites showing sampling locations relative to fractures (red lines) (Gaskill, 1991) and an alluvial fan (green polygon). (For interpretation of the references to color in this figure legend, the reader is referred to the web version of this article.)

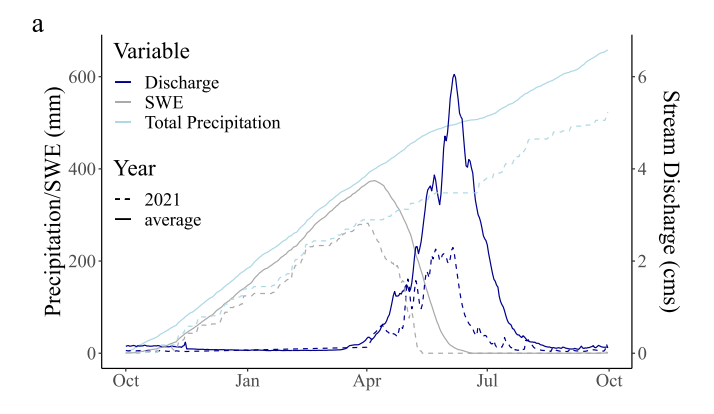
occurring in June. Flows recede throughout the summer and fall, with small peaks in flow due to monsoon events. Coal Creek reaches baseflow conditions by early September and they persist throughout the winter until the onset of snowmelt in April (Fig. 2a).

The lower portion of the Coal Creek watershed is underlain predominately by sandstone (Upper Cretaceous Mesaverde Formation) with glacial till deposits occurring near the streambed. The upper portion of the watershed is underlain by mafic intrusive plutonic rock, emplaced during the Middle Paleocene. Areas of the upper north slope of the watershed are underlain by mudstone (Tertiary Wasatch Formation) (Fig. 1b). Fractures have been mapped along the north hillslope in the upper watershed (Fig. 1b). East of the mapped fractures is the contact between the upper basin intrusive plutonic rock and lower basin sandstone. This contact roughly bisects the Coal Creek watershed running northeast to southeast. Mapped along this contact zone, on either side of Coal Creek stream, is a dense spring network (Gaskill, 1991). Alluvial fans have been mapped at the confluence of tributaries with Coal Creek.

These fans are Holocene age, poorly sorted material (Gaskill, 1991). Although many fans are present along the transect, our design only captures the alluvial fan associated with Elk Creek as our aim was primarily focused on the fracture zone compared to downstream behavior. Elk Creek is the only tributary that contributes significantly to streamflow generation along our study reach of Coal Creek throughout the summer.

2.2. Field sample collection

From June through October 2021 a total of 77 surface water samples and seven spring samples were collected for ²²²Rn and water isotopes across eight stream sites and seven springs (Table 1). Stream water sampling locations were collected along a 2842 m length reach in the upper portion of Coal Creek watershed (Table S1). Sampling locations were selected to identify the influence of mapped bedrock fractures on stream chemistry and discharge. All samples were collected in the



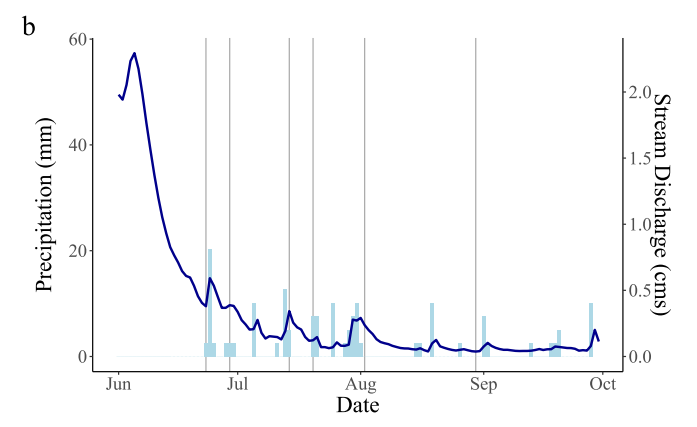


Fig. 2. (a) Average water year precipitation accumulation (left-hand axis), snow water equivalent (SWE, left-hand axis), and stream discharge (right-hand axis) in Coal Creek. Dashed lines, but same color coding, show the respective curves for the 2021 water year. (b) Precipitation events (light blue bars) and stream discharge (dark blue line) during summer sampling period (June 1- September 30, 2021). Gray vertical lines indicate sampling dates included in the model.

thalweg of the stream to ensure they were well mixed. Our study design focuses on bookending the known fracture zone along Coal Creek, with one site located just above the fractured hillslope (Upstream of Fractures, referred to as Upstream), three sampling locations located along the transect of the stream that runs along the base of the hillslope with

the mapped fractures (CC-6, CC-7, CC-8; Fig. 1B), and three samples below the fracture zone (Downstream of Fractures, referred to as Downstream; Upstream of Elk Creek, referred to as Upstream Elk; and Coal-15). We note that Upstream Elk and Coal-15 co-occur with the location of the alluvial fan at Elk Creek. Elk Creek was sampled three times throughout the summer (late May, late July, early October) at its confluence with Coal Creek, although only one sample (late July) was analyzed for ^{222}Rn . To distinguish between the behavior of the bedrock fractures and non-fracture zones, the sites can be differentiated into fracture sites (<2350 m along reach, n = 5) and non-fracture zone (>2350 m along reach, n = 2). Over 80 % of surface water samples were analyzed for both ^{222}Rn and water isotopes.

Of the seven springs, six were located on the south facing slope and one was located on the north facing slope. All but one of the springs were further east than the sampled stream reach. Each spring was sampled only once. Of the spring samples, four were analyzed for both 222 Rn and water isotopes.

2.2.1. Water sampling

Locations in a stream with high ²²²Rn concentrations indicate localized areas of groundwater discharge. ²²²Rn is not affected by biological processes and is relatively inert, although is subject to physical loss and radioactive decay. Once groundwater enters the river, ²²²Rn quickly dissipates due to degassing to the atmosphere (Schubert et al., 2020). Stream water was collected in 2L plastic bottles without headspace and spring water was collected in 500 mL plastic bottles (n = 2) or 250 mL glass bottles (n = 4) without headspace. Stream water was collected in large volume bottles to ensure accurate measurement and detection of ²²²Rn due to the relatively low concentration of ²²²Rn in stream water. Spring samples were collected in smaller bottles given the high concentration of ²²²Rn in groundwater, and were collected in different bottle types due to bottle availability at the time of sampling. Each spring was sampled only once, and one duplicate stream water sample was collected with three of the six synoptic events. All samples were collected using a Grainger surface water pump (Model IL200P, RULE, Rye Brook, NY) powered by a 12 V battery. Due to the large volume of water we needed to collect for ²²Rn analysis, we designed a sampling scheme that pumped water from the thalweg to a 2L bottle onshore. The bottle was placed in a bucket with the tubing inside, filled, and capped underwater without headspace to minimize degassing of ²²²Rn and the cap was sealed with ParafilmTM. We sampled springs similarly by placing the pump in the pool at the spring head, or as close

Table 1 Sites, times sampled, stream meter, and mean and deviation from mean (standard deviation/mean) of 222 Rn, δ^{18} O and δ^{2} H water isotope measurements.

| Site | Class | Times Sampled | Stream Meter | ²²² Rn Mean (piCL ⁻¹) | ²²² Rn Dev. from Mean (%) | δ ¹⁸ O Mean (‰) | δ ¹⁸ O Dev from Mean (%) | δ ² H Mean (‰) | δ ² H Dev from Mean (%) |
|-----------------------|------------------|------------------|-----------------|---|---|-------------------------------|--|------------------------------|---------------------------------------|
| Upstream | fracture | 7 [†] | 11,956 | 3 | 16 | -16.1 | 1.86 | -118.5 | 2.5 |
| CC-6 | fracture | 11^{\dagger} | 11,795 | 4 | 26 | -15.8 | 5.70 | -116.0 | 5.5 |
| CC-7 | fracture | 12^\dagger | 11,155 | 4 | 43 | -15.6 | 4.49 | -115.0 | 4.6 |
| CC-8 | fracture | 13^{\dagger} | 10,419 | 5 | 27 | -15.6 | 4.49 | -114.7 | 4.6 |
| Downstream | fracture | 9^{\dagger} | 9632 | 2 | 25 | -15.8 | 3.80 | -116.4 | 3.4 |
| Upstream Elk | non- fracture | 9^{\dagger} | 9221 | 12 | 46 | -15.5 | 3.87 | -114.2 | 4.0 |
| Elk Creek | non- fracture | 3^{\dagger} | 9196 | 2 | NA | -16.7 | 3.17 | -122.3 | 3.82 |
| Coal-15 | non- fracture | 13^{\dagger} | 9108 | 7 | 33 | -15.6 | 3.21 | -116.6 | 3.5 |
| Spring 1 [‡] | spring | 1 | NA | 208 | NA | NA | NA | NA | NA |
| Spring 2 | spring | 1 | NA | 619 | NA | -17.2 | NA | -125.6 | NA |
| Spring 3 [‡] | spring | 1 | NA | 651 | NA | NA | NA | NA | NA |
| Spring 4 | spring | 1 | NA | NA | NA | -17.1 | NA | -125.1 | NA |
| Spring 5 | spring | 1 | NA | 608 | NA | -16.6 | NA | -125.2 | NA |
| Spring 6 [‡] | spring | 1 | NA | 265 | NA | -17.5 | NA | -128.3 | NA |
| Spring 7 [‡] | spring | 1 | NA | 183 | NA | -17.1 | NA | -123.8 | NA |

 $[\]dagger$ Number of samples analyzed for isotope data; 222 Rn analysis was conducted two fewer times than the listed value.

[‡] Indicates ²²²Rn and water isotope samples were collected on different days and that ²²²Rn concentrations were collected in 250 mL glass vials. Unmarked spring samples were collected in 500 mL plastic bottles.

to the spring head as possible, such that the pump was completely submerged. Samples were shipped in coolers overnight to Lawrence Berkeley National Lab for ²²²Rn analysis.

Stream and spring water were also collected for stable water isotope analysis. Water samples were filtered through a 0.45-µm Nylon filter into a 2 mL glass vial with Septa caps, taking care to eliminate headspace, and refrigerated until analysis. We relied on water isotopes of precipitation collected about 10 km north-east of Coal Creek during the 2021 water year as end members to compare stream and spring water isotopic composition. Samples were collected approximately weekly, and snow (n = 23) and rain (n = 10) samples were aggregated to assess seasonal variability in precipitation (Table S2). Rain gauges were made to U.S. Weather Bureau specifications with a capacity of 27.9 cm x 2 mm. Gauges were situated in areas sheltered from winds, attempting to maintain at least two lengths of surrounding tree height to avoid turbulence. Mineral oil was used to limit evaporative effects.

2.2.2. Stream discharge

We measured stream discharge five times between June 25th and August 30th at the sites: Upstream of Fractures, Downstream of Fractures, and Coal-15 (Table S3). Starting August 3rd, discharge measurements were moved downstream from Upstream of Fractures to CC-6 because of beaver activity that dammed the Upstream site. Discharge was measured using a SonTek FlowTracker Handheld Acoustic Doppler Velocimeter. Cross sections were selected based on characteristics of straight channel, minimal boulders on stream bed, and evenly distributed flow across the channel. Due to changes in flow depth, cross section location varied throughout the summer to achieve the most accurate measurements.

2.3. Isotope sample analysis

Concentrations of ²²²Rn in the water samples were measured using a RAD7 instrument (mfd. by Durridge Co. Inc., Billerica MA). A closed loop system connected to the RAD7 (the RAD H20 for 2 L bottles -Durridge Co.) was used to sparge ²²²Rn for quantification within the instrument. After 15-minutes of sparging, counting began for 15-minute periods. After the first four counting periods (or one hour) the internal air pump of the RAD 7 was turned off, and counting continued for at least 10 counting periods, or a total counting time of at least 2.5 h. The average temperature of the water sample during the sparging process was measured using a thermo-couple electronic thermometer (Thermapen MK4. ThermoWorks, USA) held to the bottle with a Velcro strap. This temperature was used to calculate the partitioning of ²²²Rn between the air-loop and the water sample. Between sample analyses, the entire system was purged for 15 min with the atmosphere to remove ²²²Rn from the system and reduce internal humidity. Statistical pooling of the counting periods for individual analyses was conducted using Isoplot (Ludwig, 2012). Measured ²²²Rn concentrations were corrected for radioactive decay to the time of sample collection (typically measurements were analyzed < 48 hrs. post sample collection). Average analytical uncertainty was 1.2 piC/L. ²²²Rn concentrations are reported in Table 1 as pCi/L.

Hydrogen and oxygen isotope ratios of water were measured using an off-axis integrated cavity output spectrometer coupled to an autosampler interfaced with a heated injector block (Los Gatos Research, San Jose, USA). Average analytical uncertainty for hydrogen and oxygen isotopes are 0.05 and 0.14 per mil, respectively. Hydrogen and oxygen isotope ratios are reported in conventional δ notation relative to the Vienna Standard Mean Ocean Water.

2.4. Data analysis

2.4.1. Discharge, Precipitation, and evapotranspiration metrics

Mean daily Coal Creek discharge was downloaded from the USGS gage 09111250. Daily precipitation and snow water equivalent (SWE)

was downloaded from SNOTEL station 380 located on Mt. Crested Butte. Potential evapotranspiration (PET) was calculated using the Penman-Monteith equation using temperature, wind, dew point, and radiation data from the KCOCREST52 WunderGround weather station in Mt Crested Butte, Colorado. Both the SNOTEL and WunderGround stations are located outside the watershed but at the approximate elevation of the Coal Creek watershed of 3149 m (3097 m and 2913 m, respectively).

2.4.2. Seasonal origin index

The Seasonal Origin Index (SOI) is a metric that expresses the isotope signature of the stream water relative to seasonal precipitation isotope cycles (Allen et al., 2019b). The SOI was calculated for each stream water sample using the following equation:

$$SOI = \begin{cases} \frac{\delta_{x} - \delta_{mnP}}{\delta_{unmenP} - \delta_{unnP}} \\ \frac{\delta_{x} - \delta_{unnP}}{\delta_{unnP} - \delta_{winterP}} \end{cases}, \text{if } \delta_{x} > \delta_{unnP} \\ \text{if } \delta_{x} < \delta_{unnP} \end{cases}$$

$$(1)$$

where δx is the $\delta^{18}O$ isotopic signature of stream water, and $\delta_{winterP}$, $\delta_{summerP}$, and δ_{annP} are the $\delta^{18}O$ isotopic signatures of volume-weighted winter, summer, and annual precipitation at Coal Creek. The SOI is -1 when all the stream water is comprised of winter precipitation ($\delta_{winterP}$), +1 when all the stream water is comprised of summer precipitation ($\delta_{summerP}$), and 0 when the stream water isotopic composition is equivalent to the weighted average of all water year precipitation (δ_{annP}).

2.4.3. Estimation of groundwater discharge flux

Groundwater discharge flux along the fracture zone was estimated for six different stream reaches throughout the summer (6/23–8/30) using StreamTran (Smerdon and Gardner, 2022), a Python-based, one-dimensional advective–dispersive transport model that uses coupled mass balance equations of ²²²Rn concentration and discharge measurements along a transect to estimate lateral groundwater discharge into the stream. StreamTran does not account for increases in stream ²²²Rn concentration due to hyporheic exchange. The mass balance equation representing discharge is given by:

$$\frac{dQ}{dx} = Pw - Ew + \frac{Q_T}{dx} + q_{gi}w - q_{go}w \tag{2}$$

where Q (m³ s⁻¹) is stream discharge, x (m) is discretized distance downstream, P (m s⁻¹) is the precipitation rate, E (m s⁻¹) is the evaporation rate, Q_T (m³ s⁻¹) is tributary discharge, q_{gi} (m s⁻¹) is the groundwater discharge gain flux, q_{go} (m s⁻¹) is the groundwater loss flux, and w is the stream width in meters.

For 1d advective–dispersive transport of 222 Rn in the stream, including groundwater inflow, atmospheric gas exchange, and solute decay, the mass balance equation is given by:

$$\frac{dC}{dx} = \frac{d}{dx} \left(\frac{DA}{Q}\right) \left(\frac{dC}{dx}\right) + \frac{q_{gi}w}{Q} (C_{GW} - C) + \frac{Q_T}{dxQ} (C_T - C) - \frac{kw}{Q} (C - C_{ATM}) - \frac{A}{C} \lambda C$$
(3)

where C (piC L⁻¹) is the stream concentration, D (m² s⁻¹) is the longitudinal hydrodynamic dispersivity, A (m²) is the stream cross-sectional area, C_{GW} (piC L⁻¹) is the local groundwater concentration, k (m s⁻¹) is the gas exchange velocity, C_{ATM} (piC L⁻¹) is the atmospheric equilibrium concentration of the tracer, λ (s⁻¹) is the decay coefficient, and C_T (piC L⁻¹) is the tributary concentration.

2.4.3.1. Solution technique and boundary conditions. Equations 2 and 3 are fully coupled and solved using a fully implicit, finite volume method based using FiPy (Guyer et al., 2009), a python finite volume solver library. Equations 2 and 3 are solved simultaneously to estimate groundwater gain and loss along the stream reach given measured discharge, stream geometry, tributary input, precipitation, evaporation, and 222 Rn concentration. The groundwater concentration of 222 Rn,

²²²Rn gas exchange velocity, and ²²²Rn decay coefficient are required estimated parameters. The coupled equations are optimized using a Marquart-Levenberg optimization routine to minimize the chi squared residual between the observed and modeled ²²²Rn and discharge stream measurements. From these optimized equations, groundwater discharge is estimated along the transect at n equally spaced intervals, where n is equal to the number of samples.

The stream is discretized into 10,000 equally spaced approximately $^1\!/_3$ meter grids from upstream to downstream. Model unit length varied between sampling date 08/30/21 and other dates because samples from 08/30/21 began further downstream due to new construction of a beaver dam at the Upstream sampling location. Constant discharge and concentration (Dirichlet) boundary conditions are set at the upstream end of the model and set to the measured concentration and discharge at the most upstream site for a given sampling event. Constant discharge (Dirichlet) and constant concentration gradient (Neumann) boundary conditions are set at the downstream end of the model.

2.4.3.2. Parameterization. The model was parameterized to represent site conditions at the time of synoptic sampling (Table 2). Atmospheric equilibrium concentration of $^{222}\mathrm{Rn}$ was set to zero. The $^{222}\mathrm{Rn}$ decay coefficient was set to 3.82 d $^{-1}$ (Cook and Herczeg, 2000). The fully implicit finite volume technique used controls the dispersive flux in the solution even when set to zero. Therefore, longitudinal hydrodynamic dispersivity was set to zero, which means that numerical dispersion of the grid cell spacing ($\sim 1/3$ m) controls the dispersive flux (Beisner et al., 2018). Stream width and depth were measured each time discharge was measured (SI Table 1, SI Text 1) and linearly interpolated along the stream reach.

Initial ²²²Rn gas exchange velocities were calculated for each sampling event using estimated stream geometry and flow characteristics and were assumed to be constant for the length of the reach (SI Table 2). Groundwater ²²²Rn concentration was measured from six springs across the watershed. Calculated gas exchange velocities based on equations from Raymond et al., (2012) and measured groundwater ²²²Rn concentrations lead to underestimation of discharge and overestimation and ill-fitting of measured ²²²Rn concentrations (Text S3; Figures S2 and S3), which is not surprising given that gas exchange velocity and groundwater ²²²Rn concentrations are highly variable (Ulseth et al., 2019; Mullinger et al., 2009). Therefore, we used Monte Carlo simulations to estimate a range of gas exchange velocities and groundwater ²²²Rn concentrations. Gas exchange velocity is highly dependent on-stream turbulence. For high-energy, montane streams, the accuracy of

Table 2 Model input parameters.

| Parameter | Definition | Value | Note |
|------------------------|--|----------------|---|
| P | Precipitation (ms ⁻¹) | 0 | Field conditions |
| E | Evaporation (ms ⁻¹) | Table S5 | Estimated using Penman- Monteith |
| w | Width (m) | Table S4 | Stream discharge measurements |
| d | Depth (m) | Table S4 | Stream discharge measurements |
| A | Cross Sectional Area (m²) | w*d | Stream discharge measurements |
| D | Dispersivity (m ² s ⁻) ¹ | 0 | Beisner et al. (2018) |
| \mathbf{k}^{\dagger} | gas exchange velocity (ms ⁻¹) | Table 3 | Estimated using MC simulation |
| λ | Rn decay coefficient (s ⁻¹) | $4.43x10^{-5}$ | Cook and Herczeg (2000) |
| C_{atm} | Atmospheric ²²² Rn concentrations (piC/L) | 0 | Field conditions |
| C_{gw}^{\dagger} | Groundwater ²²² Rn concentrations | Table 3 | Estimated using MC simulation |
| C_{tr} | ²²² Rn concentration in Elk Creek (piC/L) | 2.1 | Field conditions, measured on July 27, 2021 |

[†] indicates parameters that varied during optimization routine.

empirical equations for estimating gas exchange velocity often diminishes. For streams with slopes similar to Coal Creek (0.029 m m⁻¹), gas exchange velocities have been observed between 1 and 100 m/ d (Ulseth et al., 2019). Monte Carlo simulations were run for each modeled sampling event using gas exchange velocities between 10 and 105 m/d (≤ 10 times estimated gas exchange velocity using empirical equations (SI Text 2)) and groundwater ²²²Rn concentrations between 100 and 600 piC L⁻¹ (approximate minimum and maximum measured spring concentrations; Table 1). A total of 3,000 Monte Carlo simulations per modeled synoptic event were run to estimate the gas exchange velocity and groundwater ²²²Rn concentration for each synoptic event. Model fit was evaluated using the Akaike Information Criterion (AIC). AIC is an estimation of prediction error, generally used to compare models and determine which is the best fit for the data (Bozdogan, 1987). Here, low AIC values indicate better fit between measured and modeled discharge and ²²²Rn concentrations. To represent a range of conditions which may give optimal model performance, we evaluated groundwater ²²²Rn concentrations and gas exchange velocities from model runs within the top 5 % of AIC values (150 runs for each synoptic event). The median values of groundwater ²²²Rn concentration and gas exchange velocity from the top 5 % simulation runs were used to parameterize the StreamTran model. Pairings of the minimum groundwater ²²²Rn concentration and minimum gas exchange velocity, and the maximum groundwater ²²²Rn concentration and maximum gas exchange velocity, from the top 5 % best models were used to characterize uncertainty around the MC estimated groundwater flux.

2.4.3.3. Discharge and stream geometry relationships. Discharge along the modeled stream reach is a required input for parameterization of StreamTran. Discharge was measured five times throughout the summer at Upstream/CC-6, Downstream, and Coal-15. Upstream and CC-6 are combined into one site because beginning August 3rd measurements had to be moved downstream from Upstream to CC-6 due to construction of a new beaver dam. These two sites are 161 m apart. Since stream discharge is responsive to monsoon rains, using measured discharge close to the sampling date is not sufficient. Thus, linear regressions between each measured site and the USGS gage data were performed to estimate discharge along the stream reach throughout the summer (Figure S1).

Width and depth were measured with discharge and are also required inputs along the stream reach. However, these parameters are responsive to changes in discharge and thus to precipitation inputs from monsoon rains. Width and depth were regressed against measured discharge (Figure S1), and those relationships were used to estimate width and depth from modeled discharge. Modeled discharge, width, and depth were used as inputs for each transect run in StreamTran (Table S5).

2.4.4. Estimation of dynamic storage

We estimated the change in dynamic storage of Coal Creek over the course of the summer using a water balance analysis. The change in dynamic storage (*dS*) was calculated as follows:

$$dS(t) = \sum_{t=1}^{T} (P(t) - Q(t) - ET(t))$$
(4)

where t is time in days (in this study t=1 on June 1, 2021), P is precipitation (mm), Q is stream water discharge (mm), and ET is evapotranspiration (mm). Actual ET measurements are not available for Coal Creek; we use PET calculated from the Penman Monteith equation in our calculations of dS. Coal Creek is a well-watered system and meets most of the assumptions required for Penman Monteith. The dS was calculated at a daily time stamp between June 1 and September 30. This water budget does not account for interbasin groundwater flow nor overland flow out of the catchment that is not routed into the stream. Although this is a simplification of the water budget, it represents the dominant processes that control water fluxes in montane catchments

(Ryken et al., 2022). Uncertainty around dS was estimated assuming a 10 % error in precipitation measurement (Larson and Peck, 1974; Ehsani and Behrangi, 2022), a 20 % error in PET relative to AET (Hua et al., 2020; Westerhoff, 2015; Kingston et al., 2009), and a 13 % error in stream water discharge calculated as the average percent difference between measured and gage-estimated discharge values for Coal Creek.

3. Results

3.1. Hydro-climatology of Coal Creek

In Coal Creek, the 2021 water year was overall drier than average, receiving only 523 mm of precipitation, compared to the average 658 mm. However, the precipitation deficit was confined predominantly to winter (October 1-March 31) and spring (April 1-June 29), where only 290 mm and 88 mm of precipitation fell, compared to the average 387 mm and 126 mm, respectively. The total amount of rain during the summer (June 30-September 30) was equivalent to the average (145 mm). The snow drought of 2021 led to 62 % lower than average peak flows (6.05 m³/s) and 57 % lower than average summer base flows (0.095 m³/s; defined as the 10th percentile flow between July 1 and September 30). Precipitation events during the summer of 2021 were generally concentrated between late June and July, with occasional precipitation events occurring through the rest of the summer (Fig. 2b).

3.2. Evaluating stream response to monsoon rains through synoptic stream chemistry sampling

3.2.1. Radon samples

Stream water $^{222}\rm{Rn}$ concentrations ranged from 2 to 20 piC/L, while spring water samples varied from 183 to 651 piC/L. The highest stream $^{222}\rm{Rn}$ was measured at Upstream Elk and the lowest was measured at Downstream of Fractures (Fig. 3). $^{222}\rm{Rn}$ was least variable at Upstream of Fractures (deviation from mean (%Dev) < 20 %), moderately variable at CC-6, CC-8, and Downstream of Fractures (20 % < %Dev < 30 %), and highly variable at CC-7, Upstream of Elk, and Coal-15 (%Dev > 30 %) (Table 1, Fig. 3).

Increasing or decreasing patterns of ²²²Rn were not temporally consistent at all sites (Fig. 4a). In general, fracture zone sites showed a decreasing trend in ²²²Rn concentration at the beginning of the summer before flattening out in July, and then increased again in late summer/early fall. Unlike the fracture zone sites, ²²²Rn concentrations at Coal-15 were low in June and increased throughout the summer before

decreasing again at the end of summer. 222 Rn concentrations at Upstream Elk were also high during summer and declined at the end of the summer. Across all sites, peaks in 222 Rn were observed in mid-July, and at the non-fractured zone sites there was an additional peak observed in mid-August. In general, peaks coincided with dry periods while lower 222 Rn concentrations coincided with periods of time with more precipitation.

3.2.2. Water isotope samples

Stream water $\delta^{18}O$ values ranged from -16.5 to -14.2 %, while spring water samples were consistently more depleted than stream water and varied from -17.54 to -16.56 % (Fig. 5). Precipitation $\delta^{18}O$ values ranged from -3.83 to -26.64 % ($\delta_{annP}=-14.67$ %); summer rain events (2021 $\delta_{summerP}=-6.95$ %) were generally more enriched than winter snow events (2021 $\delta_{winterP}=-19.56$ %). Compared to ^{222}Rn concentrations, there was less distinct spatial variation in stream $\delta^{18}O$ values.

There was a strong temporal variation in stream water isotope composition with more depleted values measured at the beginning of summer and more enriched samples measured at the end of summer (Fig. 5). In general, δ^{18} O enrichment was more pronounced in fracture zone sites than the non-fractured zone sites, with fracture zone sites becoming more enriched later in the summer in comparison to non-fractured zone sites. Across the entire stream transect in July, variability in stream δ^{18} O values were observed, where samples collected following precipitation events (e.g., 07/06, 07/14, and 07/27) had more enriched isotopic compositions and samples collected during drier periods (i.e., 07/12 and 07/20) had more depleted isotopic compositions (Fig. 4b). This suggests that during July, Coal Creek may be responding quickly to precipitation events, but this stream response was not observed in sampling events outside of July.

The patterns present in the temporal variation of $\delta^{18}O$ (Fig. 4b) are reflected in the Seasonal Origin Index (SOI) (Fig. 6). The SOI estimates the proportion of water in the stream originating as winter (snow) vs summer (rain) precipitation (Fig. 5). Within Coal Creek, SOI ranged from -0.37 to 0.06, with the most negative values observed during the earliest sampling event and the positive values observed during the latest sampling period. The variability in stream $\delta^{18}O$ composition observed in Fig. 4b is also present in Fig. 6 from dates 07/06 through 07/27. This is followed by an increase in SOI, indicating that at the beginning of the summer, stream water origin is more snow-dominated and becomes less snow-dominated throughout the summer.

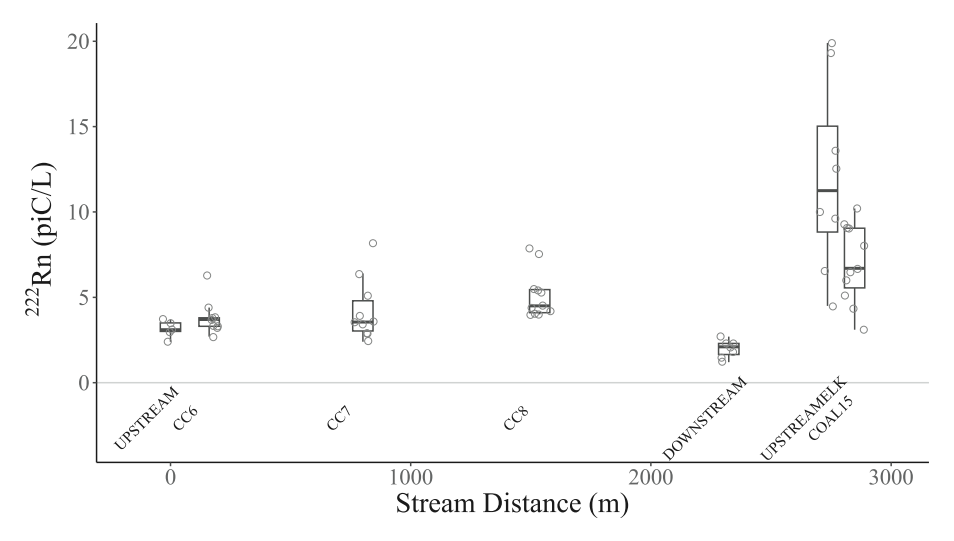


Fig. 3. ²²²Rn concentrations at surface water locations with distance downstream, not including Elk Creek. Lower and upper lines of boxplot box are quartile 1 and 3, respectively. The middle line is the median. Vertical lines indicate minimum and maximum, if less than +/- 1.5*interquartile range (IQR). Points outside +/- 1.5*IQR are considered outliers and are plotted above/below vertical lines. Open points show all samples collected on a given date.

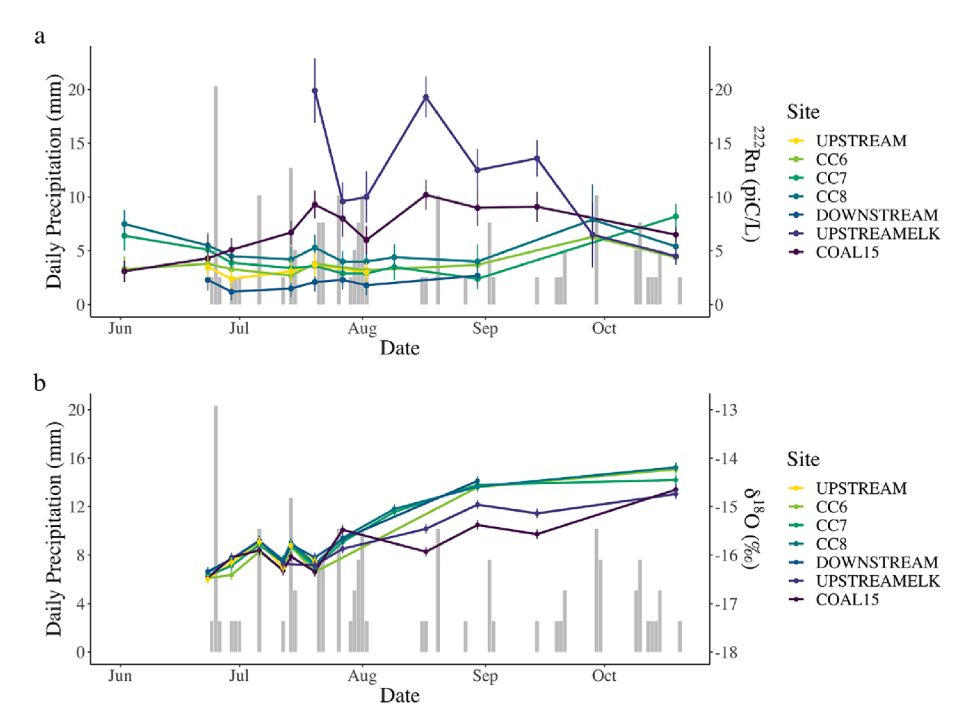


Fig. 4. (a) 222 Rn concentrations and (b) δ^{18} O values through time and analytical uncertainty (vertical lines) at sites (colored lines) as compared to the daily precipitation at Coal Creek (gray bars).

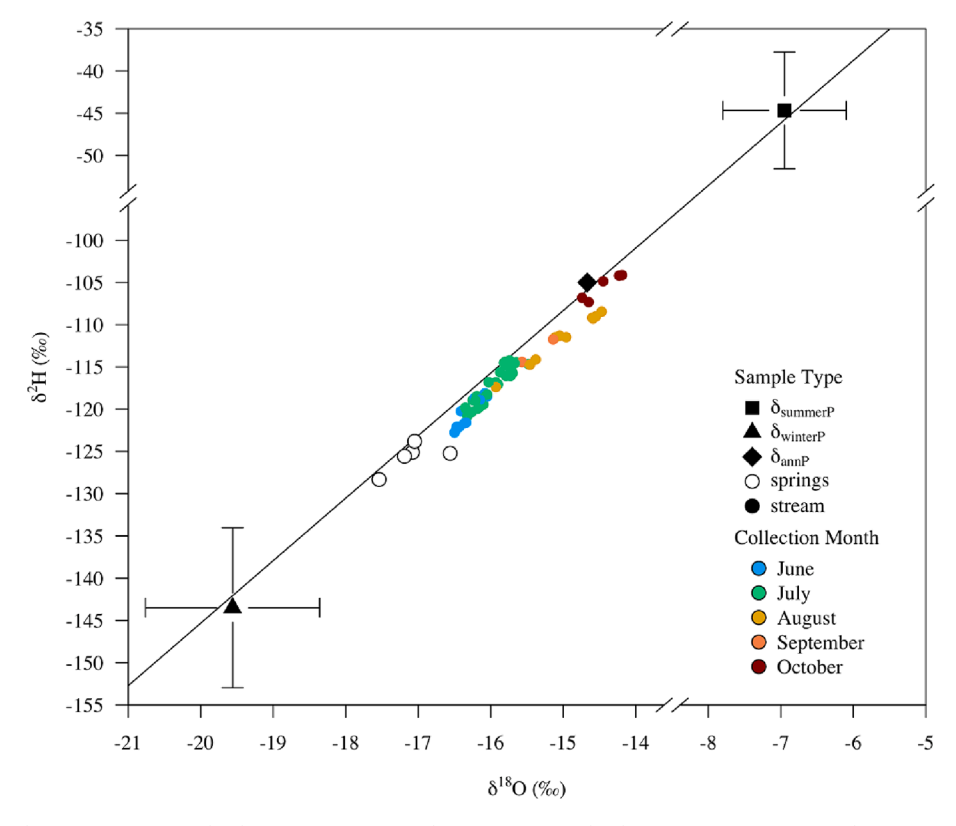


Fig. 5. Dual isotope plots showing $\delta_{winterP}$ (weighted average snow, triangle), $\delta_{summerP}$ (weighted average rain, square), and δ_{annP} (weighted average annual precipitation, diamond), spring samples (open circles), stream samples (colored circles), and the local meteoric water line (LMWL) (black line) (developed by Carroll et al., 2018). Error bars around precipitation end members indicate weighted standard errors. Colors indicate sample collection month.

3.3. Model parameterization and performance

We used the StreamTran model to estimate groundwater flux into the stream between Upstream/CC-6 and Coal-15 across six different dates $\,$

throughout the summer. Monte Carlo simulations were used to estimate the gas exchange velocity and groundwater ²²²Rn concentration for each synoptic event. Values used to parameterize each synoptic event were the median of the top 5 % best (lowest AIC) MC simulations (Table 3).

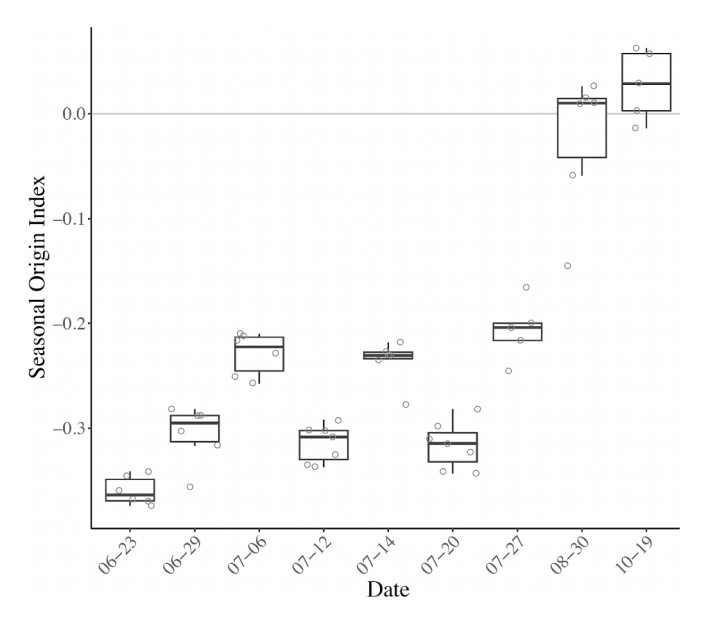


Fig. 6. Seasonal origin index (SOI) for stream samples at Coal Creek. Lower and upper lines of the boxplot box are quartile 1 and 3, respectively. The middle line is the median. Vertical lines indicate minimum and maximum, if less than +/-1.5*IQR. Points outside +/-1.5*IQR are considered outliers. Open points show all samples collected on a given date. Horizontal gray line shows SOI of 0.

Median groundwater ²²²Rn concentrations ranged from 130 to 256.5 and median gas exchange velocities ranged from 48.5 to 90. Model performance varied across modeled events, with the best performing model representing stream conditions on 07/14 (AIC = 48.08) and the worst performing model representing stream conditions on 07/20 (AIC = 73.14). Both modeled stream discharge and stream ²²²Rn concentrations generally agreed with measured values, with slight overprediction of stream discharge during 06/23, 06/29, and 07/14, and slight overprediction of stream ²²²Rn concentrations during 07/20 and 08/02.

3.4. Estimation of lateral groundwater flux through space and time

By evaluating the groundwater flux (Fig. 8) we can quantitatively evaluate how groundwater discharge varied in space and time. There were two distinct spikes in GW flux along the fractured zone and consistently high GW flux in the non-fractured zone (Fig. 8). We categorized two different temporal behaviors: early summer (06/23–07/14) and late summer (07/20–08/30). In general, during early summer, groundwater contributions between both the fractured and non-fractured zones were similar. The highest flux from the fractured zone and lowest flux from the non-fractured zone occurred on 06/23 and the lowest flux from the fractured zone and highest flux from the non-fractured zone occurred on 07/14. There was similar spread between all three early summer sampling dates across both the fractured and non-fractured zone. In contrast, during late summer, groundwater contribution from the fractured zone was lower than that from the non-

Table 3 Median output from top 5% Monte Carlo simulation runs for groundwater 222 Rn concentrations and gas exchange velocity (GEV) for the six model dates. Final model AIC is shown as well.

| Date | Median ²²² Rn (piC/L) | Median GEV (m/d) | Final Model AIC |
|-------|----------------------------------|------------------|-----------------|
| 06/23 | 139.5 | 90.0 | 59.03 |
| 06/29 | 130.0 | 86.5 | 54.98 |
| 07/14 | 137.0 | 84.0 | 48.08 |
| 07/20 | 256.5 | 48.5 | 73.14 |
| 08/02 | 188.5 | 73.0 | 65.73 |
| 08/30 | 245.5 | 77.5 | 60.08 |

fractured zone fan, and contribution from the fractured zone was more variable compared to the non-fractured zone contribution.

To convert to groundwater discharge, flux was multiplied by the average width of the stream and 0.3 m, which is the length of one discretized model unit. Cumulative groundwater discharge shows a similar divide between early and late season sampling events (Fig. 9a). Early summer events show a larger absolute groundwater discharge and steeper and steadier slope in groundwater discharge over the stream transect than late season events. Late season events show a flatter slope in the upper portion of the stream transect, indicating less groundwater discharge across the fracture zone, with a similar slope when compared to early season sites along the non-fractured zone.

Across the six dates, the proportion of groundwater contribution to increase in flow across the modeled reach ranged from 60 % on August 2 to 95 % on August 30 (Fig. 9b). Water from the fracture zone contributed between 35 % and 77 % of total groundwater with the highest proportional contribution early in the summer. Water from the non-fractured zone contributed between 23 % and 65 % of total groundwater with the highest proportional contribution later in the summer (Fig. 9b). Fracture zone contributions declined both volumetrically and proportionally throughout the summer whereas non-fractured zone volumetric contributions stayed relatively constant and increased their proportion.

3.5. Relating dynamic storage to SOI and groundwater discharge

We evaluated how catchment storage changed over the course of the summer using changes in daily dynamic storage. Dynamic storage was highest during the beginning of the summer and lowest at the end of the summer (Fig. 10a). Over the course of the sampling period used for modeling (6/23/21 to 8/30/21) dynamic storage declined by 176 mm, indicating significant draining of the dynamic storage zone throughout the summer. We evaluated the relationship between dynamic storage and SOI, cumulative groundwater discharge, and the ratio of fractured zone to non-fractured zone groundwater discharge across the six modeled sample dates (Fig. 10). We found significant relationships between dynamic storage and all three parameters, indicating that periods of higher connectivity (i.e., higher dynamic storage) are associated with more snow dominated streamflow and more groundwater discharge, specifically originating from the fractured zone, into Coal Creek.

4. Discussion

Changing subsurface connectivity driven by variable moisture conditions is well documented across diverse watersheds (Blume and van Meerveld, 2015; Covino, 2017). Hydrologic connectivity describes how deep and shallow groundwater link to surface water, where in highly connected watersheds streamflow is typically older and groundwater is typically more important for streamflow generation (Kirchner, 2009; Ajami et al., 2011; Heidbüchel et al., 2013; McIntosh et al., 2017). Thus, systems with lower connectivity typically rely on water in the shallow, or dynamic, storage zone. Dynamic storage is part of overall catchment storage and defined as the variation in storage between wet and dry periods (Spence, 2007; Kirchner, 2009; Sayama et al., 2011; Dwivedi et al., 2019). Previous work at Coal Creek suggests that deep storage in the basin is low, and the stream is supplied mostly from water originating in the dynamic storage zone (Zhi et al., 2019; Johnson et al., 2023). During the summer of 2021, we sampled seven springs to capture diverse groundwater chemistry across the catchment, yet median sampled spring chemistry showed ²²²Rn concentrations three times higher than median modeled contributing groundwater concentrations. This discrepancy in chemical signature between modeled groundwater chemistry and spring samples indicate that deeper groundwater is not a major contributor to the stream. Rather, streamflow generation at Coal Creek is dependent on shallow flow paths that propagate through the dynamic storage zone.

We used dynamic storage to understand subsurface connectivity,

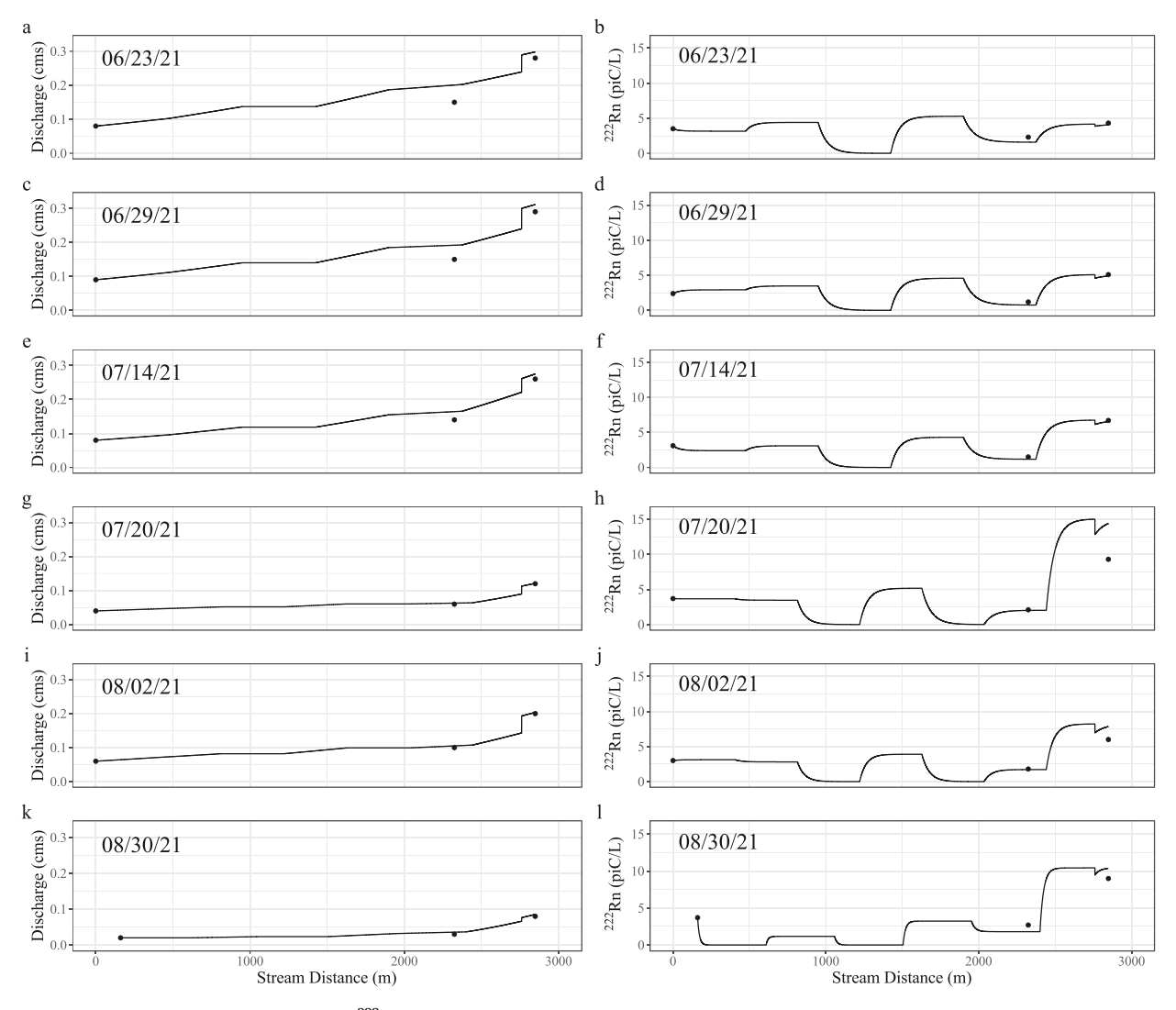


Fig. 7. Stream discharge (a, c, e, g, i, k) and stream 222 Rn concentration (b, d, f, h, j, l) measurements (points) compared to StreamTran modeled values (line) along the stream reach.

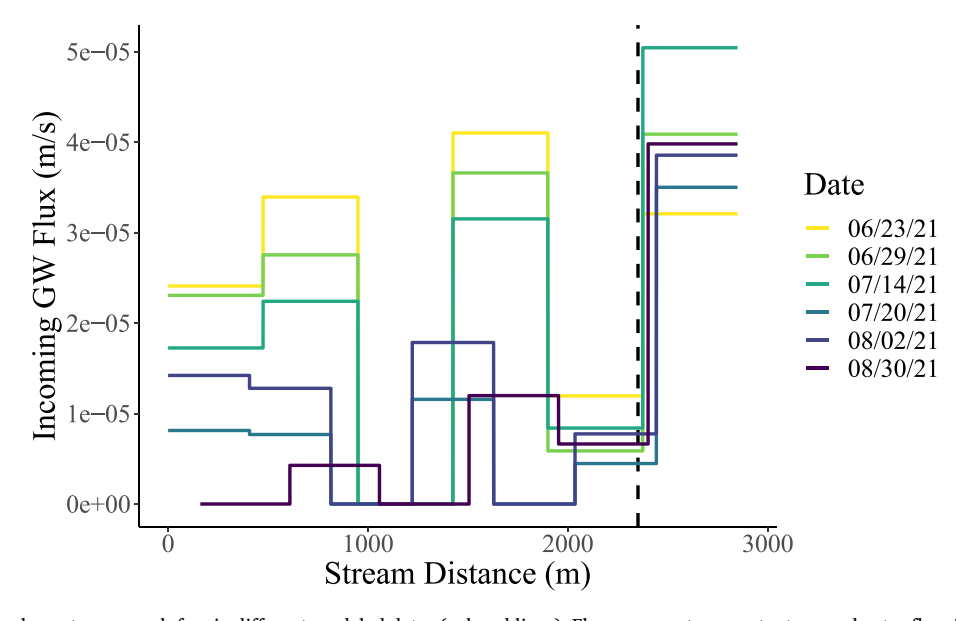


Fig. 8. Groundwater flux along stream reach for six different modeled dates (colored lines). Flux represents a constant groundwater flow into the stream along each discretized section. Dashed line indicates the transition from the fractured zone to non-fractured zone.

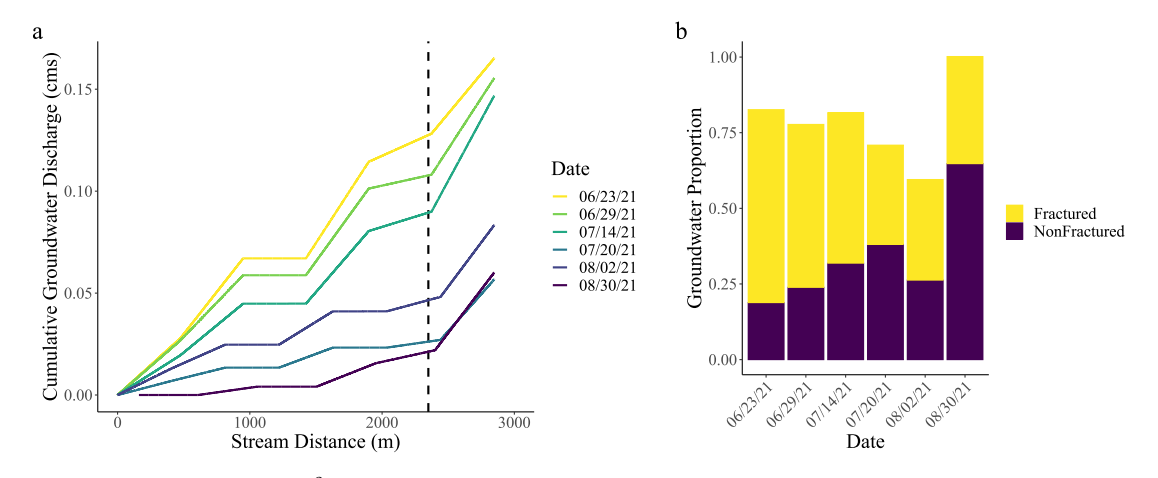


Fig. 9. (a) Cumulative groundwater discharge (m³/s) along Coal Creek for six different modeled dates (colored lines). This assumes that groundwater discharge above the most-upstream-sampled location was zero. The dashed line indicates the transitions from fractured to non-fractured zone (2350 m). (b) The proportion of increase in flow between Upstream/CC-6 and Coal-15 attributed to groundwater for the six different modeled dates colored according to the amount contributed from the fracture zone (<2350 m, yellow) and the non-fractured zone (<2350 m, deep purple). (For interpretation of the references to color in this figure legend, the reader is referred to the web version of this article.)

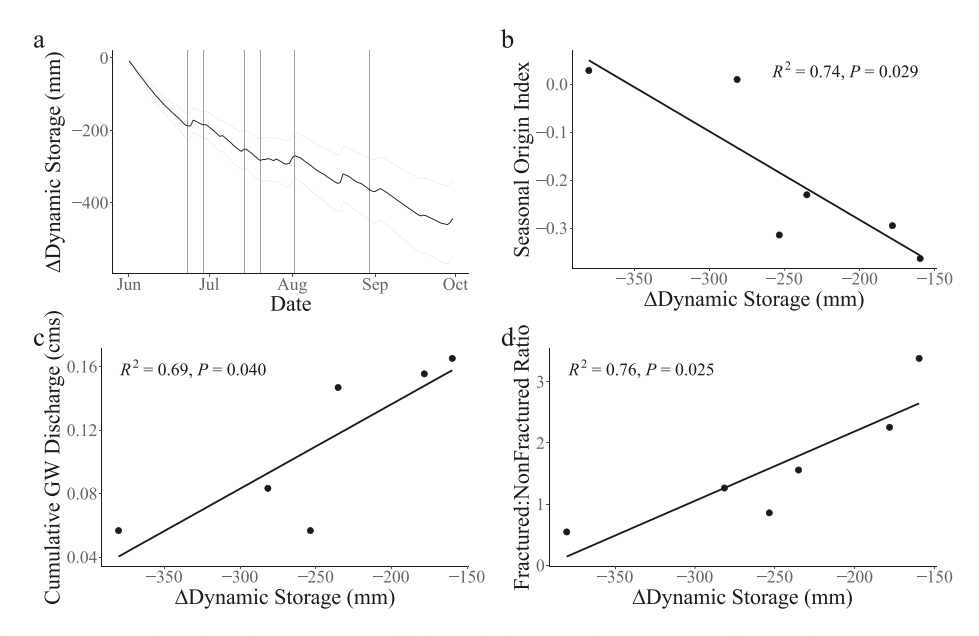


Fig. 10. (a) Change in dynamic storage throughout the summer. Modeled sample dates are shown as vertical lines and uncertainty around the calculated dynamic storage value is shaded grey. Panels b-d show the relationships between change in dynamic storage and (b) seasonal origin index, (c) mean groundwater flux, and (d) the ratio of fractured zone to non-fractured zone groundwater discharge. R² and p-values for each relationship are shown in the respective panel. All relationships are significant at the 0.05 level.

where periods of high dynamic storage are associated with high subsurface connectivity. Our results indicate that as the dynamic storage zone drains (i.e., high to low dynamic storage) throughout the summer, Coal Creek transitions from a high to low hydrologically connected system, relying more on shallow flow paths for streamflow (Fig. 10a). This hypothesis is supported by water isotopic evidence that indicates a shift in the stream water source from snow dominance to a higher share of rain in Coal Creek throughout the summer (Fig. 6), reductions in the responsiveness of groundwater discharge to the stream following precipitation events (Fig. 4), and correlations between dynamic storage and SOI and GW discharge (Fig. 10). Interestingly, despite the overall low storage and low connectivity of Coal Creek, groundwater inputs and isotopic responses along Coal Creek varied spatially and were related to changes in storage (Fig. 8, Fig. 10). These findings are discussed below in detail.

4.1. Stream water origin signals short residence time flow paths dominate in Coal Creek

Coal Creek stream water origin shifts from more to less snow dominated throughout the summer, with values of SOI ranging from -0.37 to just above 0 (Fig. 6). These values are similar to those observed in other monsoon-impacted and montane sites. For example, in the Xiangjiang River basin, China, SOI values ranged between -0.5 and 0 and progressively increased throughout the summer (Xiao et al., 2022). This suggests that summer precipitation in the Xiangjiang River basin is preferentially partitioned to ET, leaving predominantly winter precipitation to feed streamflow. However, SOI values have also been shown to exhibit more dramatic seasonal shifts, exemplified by Allen et al., (2019a) across Swiss catchments. Here SOI values ranged from -1 to 1, indicating that more summer precipitation becomes streamflow in these catchments compared to Coal Creek.

At Coal Creek, summer precipitation plays an increasingly important role in streamflow generation during dry periods and later in the summer (Fig. 6). The increased reliance on summer precipitation for streamflow reflects a shift towards shallower flow paths driven by a decline in connectivity (Covino, 2017). We found a significant, negative relationship between SOI and dynamic storage, indicating that as dynamic storage drains (i.e., more negative dynamic storage values), SOI increases indicating a shift in stream water source towards a higher proportion of rain (Fig. 10b). Shifting stream water source throughout the summer is well documented, with many catchments showing shifts towards deep groundwater (Rademacher et al., 2005; Żelazny et al., 2011a,b), and some showing shifts towards shallower flow paths (Spencer et al., 2021; Bush et al., 2023). In catchments impacted by the North American monsoon, summer precipitation can be important for streamflow generation (Carroll et al., 2020). However, when ET demand is high, summer precipitation is often preferentially partitioned to plant uptake (Julander and Clayton, 2018), leading to winter precipitation dominating summer stream flows (Sprenger et al., 2022; Xiao et al., 2022). For Coal Creek, increasing, but still negative, SOI values later in the summer indicate that although summer precipitation becomes more important throughout the summer, streamflow is still snow-dominated suggesting summer precipitation may be partitioned towards ET and away from stream flow generation.

Interestingly, we observed stream responses to incoming precipitation during periods of higher dynamic storage as well. In general, higher SOI values and more enriched δ^{18} O values in stream water followed precipitation events in early summer (Fig. 4b, Fig. 5). It is well documented that precipitation can infiltrate quickly into the subsurface and, in highly permeable areas, discharge into the stream (McDonnell, 1990; Wittenberg et al., 2019). We do not observe this quick stream response to precipitation later in the summer, yet we observe an overall enrichment of stream $\delta^{18}O$ values and SOI. We hypothesize that this quick stream response to precipitation is facilitated by rainfall moving through the bedrock fractures during periods of high connectivity, which become disconnected from the stream during periods of low connectivity and therefore no longer transport precipitation to Coal Creek. Later in the summer, precipitation transport leading to enriched values of δ^{18} O, and more positive SOI values, may originate from shallow flow paths connected to the stream in high storage areas, such as the non-fractured zone. Overall, our results suggest that the low-storage fractures respond quickly to incoming precipitation during periods of high connectivity whereas high-storage areas of the catchment may facilitate consistent transport of both summer precipitation through shallow flow paths and snowmelt-recharged groundwater through deeper flow paths.

Climate predictions suggest that snowmelt will occur earlier (Clow, 2010; Kapnick and Hall, 2012) and that the onset of monsoon rains will occur later (Cook and Seager, 2013) with warming, leading to longer summer dry periods. At Coal Creek, where monsoon rains play an important role in sustaining late summer flows, the shift in summer precipitation onset and timing may lead to lower summer flows. In addition, increased ET (Mastrotheodoros et al., 2020; Milly and Dunne, 2020) may partition more precipitation away from streamflow generation leading to further reductions in stream flow. With warming, groundwater is expected to become more important for summer stream flows because of shifts in precipitation and melt timing (Mayer and Naman, 2011; Ficklin et al., 2013; Segura et al., 2019), however in catchments like Coal Creek lacking contributions from deep storage, localized groundwater inputs from high storage features can provide significant amounts of flow to streams in the summer (Käser and Hunkeler, 2016) and buffer declines in moisture throughout the summer (Herron and Wilson, 2001). Therefore, evaluating how local geology responds to changes in connectivity is critical for understanding how Coal Creek streamflow may respond under warming conditions.

4.2. Groundwater contribution from fracture vs non-fracture zones show distinct temporal variability

We evaluated the spatial variability in connectivity along the Coal Creek transect through both groundwater flux estimates and responsiveness to incoming precipitation. Groundwater flux values ranged from 0 to 5 x 10^{-5} m s⁻¹, and generally declined throughout the summer as dynamic storage decreased (Fig. 8, Fig. 10c). Flux values (0 to 5 x 10^{-5} m s⁻¹ or 0 to 1.3 m³ m⁻¹ d⁻¹ (linear discharge at model unit width 0.3 m) fall within the range of estimated groundwater fluxes from other applications of this model. This paper is the first application of StreamTran in a montane region, but linear discharge estimations from the Fitzroy River, Australia varied between 0 and 0.5 m³m⁻¹ d⁻¹ (Gardner et al., 2011), and in the Daly River, Australia linear discharge varied between 0 and nearly 200 m³ m⁻¹ d⁻¹(Smerdon et al., 2012). Higher groundwater discharge has been observed along reaches near springs, where deeper, regional groundwater discharges to streams (Smerdon et al., 2012; Beisner et al., 2018). In contrast, reaches with lower discharge but more consistent groundwater contribution may reflect the presence of faults and onlapped geology giving rise to permeable preferential flow paths (Gardner et al., 2011), functioning similar to the fractures in Coal Creek.

In Coal Creek, groundwater contributed between 60 % and 93 % of increased flow between the start and end of the modeled reach. The fracture zone contributed between 36 % and 77 % and the non-fractured zone contributed between 23 % and 64 % of groundwater influx (Fig. 9). Groundwater flux through the fracture zone was highest during early summer when the subsurface was saturated from snowmelt and most hydrologically connected (Fig. 8). As connectivity declined throughout the summer, groundwater fluxes through the fractures and the proportion of fracture zone contributions also declined. Studies that have evaluated how fracture flow changes with moisture conditions have found shallow fractured bedrock is highly sensitive to changes in seasonal moisture (Salve et al., 2012) and that fracture flow is significantly slower during periods of lower moisture (Flerchinger et al., 1993). In contrast, groundwater flux through the non-fractured zone was constant throughout the summer, regardless of subsurface connectivity. We used a ratio of fracture zone groundwater flux to non-fractured groundwater flux to evaluate how groundwater contribution from different features changed as connectivity declined and found a strong, significant, positive relationship between fractured: non-fractured groundwater flow and dynamic storage (Fig. 10d). The fracture: non-fractured groundwater ratio ranged from >3 to <1 and declined as dynamic storage declined indicating that during periods of high connectivity the fracture zone was contributing over three times as much water as the nonfractured zone. In contrast during periods of low connectivity, the non-fractured zone contributed more than double what the fracture zone contributed indicating that this zone becomes a more important source of streamflow when dynamic storage is low. This indicates that groundwater in the non-fractured zone may be originating from an area with high subsurface storage that is hydraulically connected to the stream during periods of low connectivity (Fig. 11).

Further evaluation of the local geology in the non-fractured zone revealed an alluvial fan at the base of Elk Creek, a perennial tributary to Coal Creek, which may facilitate the transport of water through the subsurface into the stream. Two known hydrologic factors could control subsurface flow through the alluvial fan: 1) water from Elk creek is recharging the alluvial fan and then discharges into this zone, and 2) the alluvial fan is storing and discharging water from a different source than Elk Creek. If water were directly being recharged from Elk Creek through subsurface flow paths, we would expect that the sampling sites in the non-fractured zone would have an isotopic signature that reflects mixing of upstream waters with Elk Creek over time, proportional to the contribution of water from the fractured vs non-fractured zone (Fig. 9b). StreamTran model output indicates that groundwater contribution from the fan becomes increasingly important throughout the summer; if water

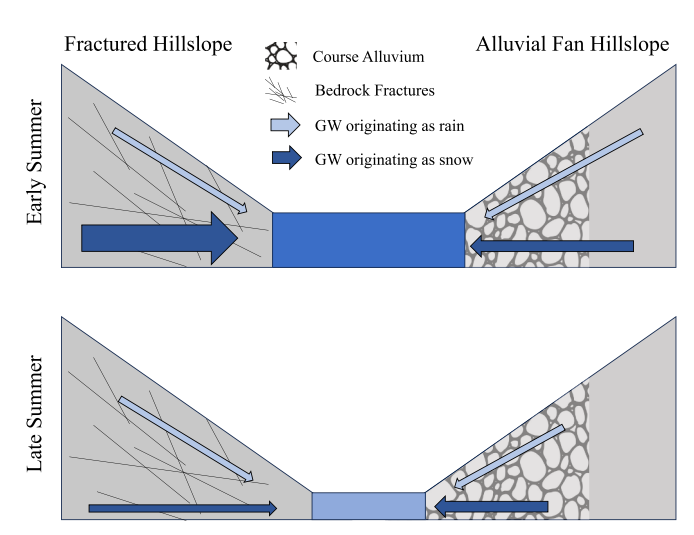


Fig. 11. Conceptual diagram developed based on SOI that depicts groundwater originating from snow and rain recharging stream water under fractured and alluvial fan hillslopes during early and late summer. In early summer, groundwater that originated from snow ($\delta_{winterP}$) dominated the fractured hillslope, while in late summer groundwater flow declined and was equally composed of snow and rain. Unlike the fractured hillslope, groundwater that originated from the alluvial fan was consistent in volume and its snow-dominated composition. Early in the summer, the alluvial fan and area upslope of the fan contributed groundwater to the stream, while later in the summer the upslope became disconnected and the alluvial fan was the dominant water source. Overall, stream water composition moved from greater snow ($\delta_{winterP}$) origin in early summer to greater rain origin ($\delta_{summerP}$) in late summer. Height of the arrows indicate the relative proportion of groundwater that originated from rain or snow to the stream

from the fan was originating from Elk Creek, we would expect that the water at the Upstream Elk location would appear chemically similar to Elk Creek, especially later in the summer. Elk Creek remains depleted throughout the summer (δ^{18} O mean = -16.7, δ^{18} O SD = 0.5) whereas Upstream Elk becomes more enriched throughout the summer (Fig. 4b). Additionally, Coal-15, the site downstream of Elk Creek, is consistently more depleted than the Upstream Elk site (Fig. 4b), indicating that the water coming into Coal Creek from Elk Creek is more depleted than that of the water entering through the alluvial fan. We therefore conclude that the alluvial fan is storing water chemically different than Elk Creek.

Water flowing through the alluvial fan shows similar isotopic composition to fracture zone water during early summer (i.e., June and July) but begins to deviate starting in August, showing a more depleted signature than fracture zone samples. This suggests that alluvial fan groundwater may be originating from deeper flow paths, transmitting isotopically depleted snowmelt into the stream later in the summer due to high storage and hydrologic connectivity associated with the fan (Fig. 11). The high connectivity of the fan would allow for transport of groundwater into the stream throughout the summer, consistent with the patterns observed in model output. This behavior is consistent with other studies quantifying the groundwater contribution of alluvial fans to streams; fans have been shown to contribute significant amounts of water to streams (Liu et al., 2004; Gordon et al., 2015), especially during low flow periods (Käser and Hunkeler, 2016).

4.3. Modeling limitations and future work

Our work points towards a need to understand localized ground-water contributions in montane environments, especially those that rely on monsoonal precipitation for summer stream flow generation. While the methods presented in this paper allow for both data driven and modeling analysis of GW-SW interactions, there are several important limitations to consider. The largest sources of error in our model are

groundwater ²²²Rn concentration and gas exchange velocity. Throughout the summer, we measured chemistry from seven springs to capture diverse groundwater behavior, yet when used in the model to predict stream flow and chemistry, modeled stream chemistry drastically diverged from measured stream chemistry. Thus, we concluded that groundwater feeding the springs was not the same groundwater directly contributing to Coal Creek. Gas exchange velocity can be measured using tracer injection tests (Wanninkhof et al., 1990; Maurice et al., 2017), however no tracer test was performed for this work. We used Monte Carlo (MC) simulations to estimate both the groundwater ²²²Rn concentration and gas exchange velocity. MC bounds for gas exchange velocity were set based on gas exchange literature values for streams of similar size and slope as Coal Creek (Raymond et al., 2012; Ulseth et al., 2019). As expected, gas exchange values varied with discharge, with higher gas exchange values estimated during higher flow periods and lower gas exchange values measured during lower flow. Bounds were set for groundwater ²²²Rn concentration based on the minimum and maximum ²²²Rn concentration measured in springs in the watershed. From the MC simulations, groundwater ²²²Rn concentrations were generally estimated to be low relative to measured ²²²Rn concentrations, suggesting that groundwater contributing to Coal Creek was relatively young (<1 week).

Gas exchange velocity and groundwater ²²²Rn concentration parameters exert opposite effects on stream water concentrations: higher gas exchange velocities reduce instream ²²²Rn concentrations whereas higher groundwater ²²²Rn concentrations increase instream ²²²Rn concentrations. We evaluated the relationship between estimated gas exchange velocities and groundwater ²²²Rn concentrations and found they were negatively correlated and, as expected, gas exchange velocity was positively related to discharge (Figure S4). The median of gas exchange and groundwater ²²²Rn concentration values across the top 5 % best model runs were used to calibrate StreamTran. Pairings of the minimum groundwater ²²²Rn concentration and minimum gas exchange velocity, and the maximum groundwater ²²²Rn concentration and maximum gas exchange velocity from the top 5 % best models were used to characterize uncertainty around the MC estimated groundwater flux (Table S6). While there was variability in estimated GW flux across the range of values retained in the top 5 % of AIC values (Fig. 12), declining trends in groundwater flux throughout the summer and variability across the reach exceeded uncertainty. Visual inspection of model output using MC estimated values showed a good fit between measured and modeled stream discharge (Fig. 7), however, near stream piezometers and tracer injection tests likely would have provided better constraints on values for groundwater ²²²Rn concentrations and gas exchange velocity.

In StreamTran, estimations of groundwater flux and stream water $^{222}\mathrm{Rn}$ concentrations are sensitive to the distance between sampling locations. Groundwater ²²²Rn degasses upon contact with the atmosphere, and in small streams with high gas exchange velocity, changes in ²²²Rn can happen rapidly. The scale length describes how far apart samples should be taken given discharge and stream geometry (Cook et al., 2006). Scale lengths in Coal Creek vary between 28 and 101 m depending on stream reach location and discharge but are shorter than the distances between samples we used (161-787 m). We acknowledge that this sample design may lead to an underestimation of groundwater inputs, especially in the portion of the reach further upstream from sampling locations. However, the goal of using this model was to compare how spatial groundwater discharge varied across time. While the reach length is longer than the length scale, the sampling locations were held constant across the sampling events and therefore we are still able to look at differences with time and interpret changes between events.

In addition to limitations imposed by data availability, StreamTran has several assumptions that influence the predicted volume of groundwater discharge. StreamTran does not consider hyporheic exchange, which can contribute substantial amounts of ²²²Rn to streams

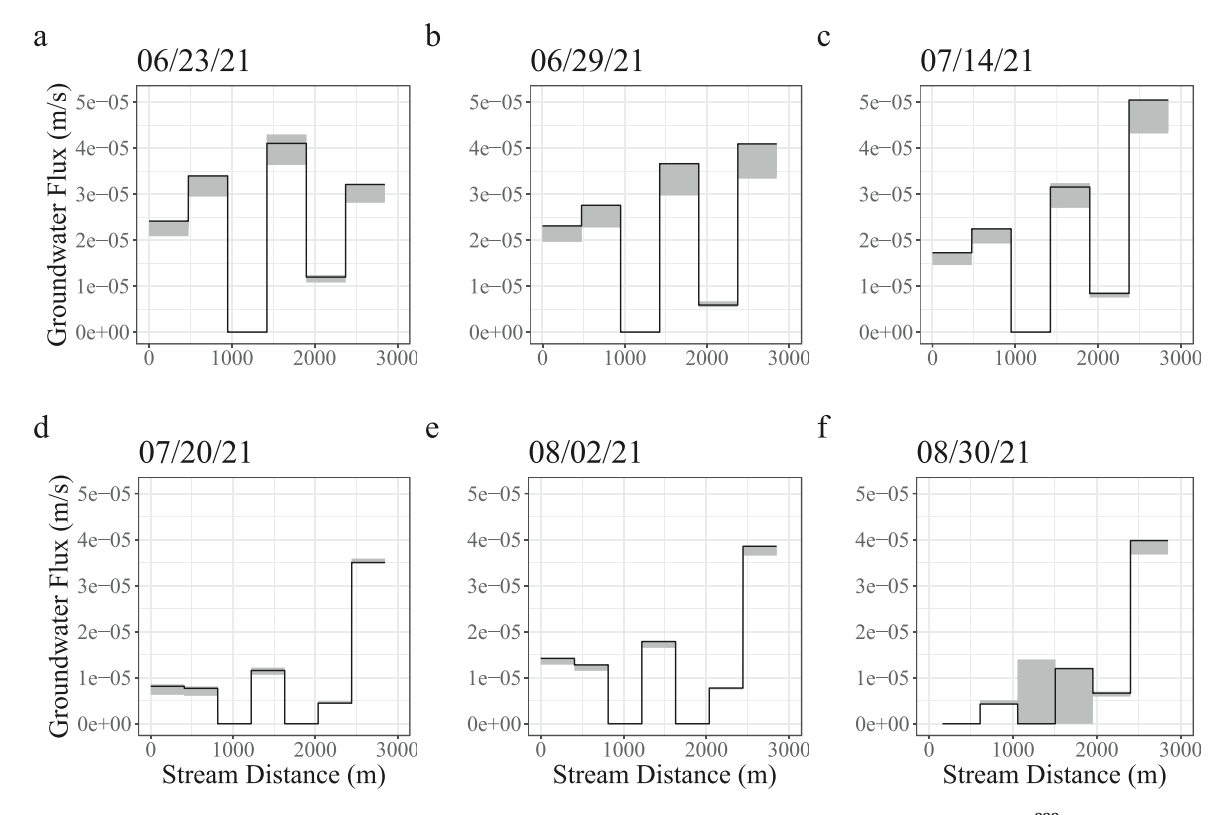


Fig. 12. Modeled groundwater fluxes (black line) and uncertainty (grey shading) estimated using the minimum paired groundwater ²²²Rn and gas exchange velocity, and maximum paired groundwater ²²²Rn and gas exchange velocity from the top 5% of AIC values from the Monte Carlo analysis for each modeled event.

(Cook et al., 2006; Bourke et al., 2014; Cartwright and Hofmann, 2016). Hyporheic exchange describes the exchange of stream water through alluvial aquifers through flow paths that begin and end in the stream channel (Gooseff, 2010). While we acknowledge that the omission of hyporheic exchange in our model may lead to overestimations of groundwater flux, along reaches longer than hyporheic flow paths (i.e., cm to tens of meters) (Boano et al., 2014), hyporheic exchange does not increase total stream flow. Along our modeled reach, streamflow increases substantially with limited input from tributaries, indicating groundwater contributions must be driving flow increases. StreamTran accounts for the gaining nature of the reach by fitting not only ²²²Rn concentrations but also measured discharge. Therefore, the model fit is weighted toward groundwater discharge that increases stream flow, and we can be confident that increasing streamflow and peaks in ²²²Rn concentration indicate groundwater contribution and not Rn input from hyporheic exchange. Additionally, the groundwater fluxes estimated by the model are used for comparison over time; evaluating relative differences among synoptic events is valid even if estimations are high.

StreamTran assumes steady state conditions of spatially and temporally input parameters, including stream temperature, evaporation, gas exchange velocity, groundwater ²²²Rn concentration, and stream slope. It is well documented that groundwater $^{222}\!\mathrm{Rn}$ concentration can be spatially variable at Coal Creek (Table 2) and in other streams (McClymont et al., 2012; Floriancic et al., 2018). Gas exchange velocity is influenced by factors such as turbulence, depth, slope, and stream temperature that vary across the modeled stream reach. Finally, StreamTran uses a linear interpolation of width, depth, and area and assumes a rectangular stream channel between measurement locations which erases much of the complex channel morphology present in small headwater streams (Schneider et al., 2015). When we included temporal variation of all input parameters between sampling dates using the Monte Carlo approach, we observed that patterns in modeled groundwater discharge in time and space outweigh the uncertainty introduced by steady state behavior (Fig. 12). With similar datasets, this could be applied to other river systems (Beisner et al., 2018) to understand localized and regional groundwater contribution to streamflow.

Future work at Coal Creek could leverage this new model of groundwater flow to understand solute transport. The Coal Creek watershed, and many other watersheds in the Rocky Mountains, are heavily mined and mineralized leading to concerns about metal transport into streams. Coal Creek serves as the drinking water supply for the town of Crested Butte, and previous work has identified high concentrations of zinc, cadmium, and copper in stream water (Manning et al., 2008; Verplanck et al., 2010). A better understanding of fracture and alluvial fan groundwater contributions may help elucidate source and timing of metal fluxes into Coal Creek.

5. Conclusion

Understanding local controls on GW-SW interactions is critical as groundwater becomes more important for summer streamflow generation under warmer conditions. We used spatial and temporal $^{222}\!\mathrm{Rn}$ and water isotope sampling along a three km reach of a Colorado River headwater stream to assess how bedrock fractures control GW-SW interactions throughout the summer. The model application presented here is transferable to other stream reaches with similar geochemistry data to understand how streamflow generation processes shift through time and space. We characterized changes in subsurface hydrologic connectivity throughout the summer using dynamic storage, and found the catchment shifts from high to low hydrologic connectivity over the summer. We observed variable responses to declining connectivity between geologic features. During early summer, groundwater contributions through the fracture zone dominated groundwater flux along the reach but declined as summer progressed. In contrast, groundwater contributions from the non-fractured zone were constant throughout the study and dominated in late summer when fracture contributions were low. We hypothesize that groundwater in the non-fractured zone is dominantly sourced from a high-storage alluvial fan at the base of Elk

Creek that is connected to Coal Creek throughout the summer and provides consistent groundwater influx. Throughout the summer, streamflow origin shifted from more to less snow dominated reflecting the important role that monsoonal precipitation plays in streamflow generation during the late summer. At the catchment scale, we observed significant relationships between dynamic storage and water isotope values, groundwater discharge, and the ratio of fractured to nonfractured zone groundwater contribution indicating that periods of higher connectivity led to more snow dominated stream water, higher groundwater discharge, and a higher proportion of fracture zone groundwater in Coal Creek. Overall, we observed that shallow flow paths became more important for streamflow generation during low hydrologic connectivity conditions, but local geologic features responded differently to changes in moisture based on their storage. Under warmer conditions, groundwater and monsoon rains may become more important for sustaining summer flows. Based on this work, we expect high storage features, such as alluvial fans, to become more important for sustaining streamflow under warming. Additionally, we expect a higher proportion of late season streamflow to originate from monsoon rains transported through shallow flow paths as deeper groundwater transported through low storage features may become disconnected from the stream earlier in the summer. To better understand streamflow generation processes in montane catchments, additional assessment of groundwater and stream response to warming and monsoon rain is

CRediT authorship contribution statement

Keira Johnson: Writing – review & editing, Writing – original draft, Visualization, Investigation, Formal analysis, Data curation, Conceptualization. John N. Christensen: Writing – review & editing, Resources, Investigation, Formal analysis, Conceptualization. W. Payton Gardner: Writing - review & editing, Supervision, Software, Resources, Methodology, Investigation, Formal analysis. Matthias Sprenger: Writing review & editing, Formal analysis. Li Li: Writing - review & editing. Kenneth H. Williams: Writing - review & editing, Project administration, Investigation, Funding acquisition, Conceptualization. Rosemary W.H. Carroll: Writing - review & editing, Investigation. Nicholas Thiros: Writing - review & editing, Investigation. Wendy Brown: Writing - review & editing, Resources. Curtis Beutler: Writing - review & editing, Investigation. Alexander Newman: Writing - review & editing, Investigation. Pamela L. Sullivan: Writing – review & editing, Writing – original draft, Visualization, Supervision, Resources, Funding acquisition, Formal analysis, Conceptualization.

Declaration of competing interest

The authors declare that they have no known competing financial interests or personal relationships that could have appeared to influence the work reported in this paper.

Data availability

Code is available on Zenoto. Data is available on ESS-DIVE

Acknowledgements

This material is based upon work supported by the National Science Foundation under Grant No. (PL Sullivan: NSF 2034232, and 2012796) and the Department of Energy under Grant No. (PL Sullivan + L Li: DESC0020146). K.H.W., J.N.C., R.W.H.C and M.S. are supported by the US Department of Energy Office of Science under contract DE-AC02-05CH11231 as part of Lawrence Berkeley National Laboratory Watershed Function Science Focus Area.

Appendix A. Supplementary data

Supplementary data to this article can be found online at https://doi.org/10.1016/j,jhydrol.2024.131202.

References

- Ajami, H., Troch, P.A., Maddock III, T., Meixner, T., Eastoe, C., 2011. Quantifying mountain block recharge by means of catchment-scale storage-discharge relationships. Water Resour. Res. 47 (4) https://doi.org/10.1029/2010WR009598.
- Allen, S.T., Kirchner, J.W., Braun, S., Siegwolf, R.T.W., Goldsmith, G.R., 2019a. Seasonal origins of soil water used by trees. Hydrol. Earth Syst. Sci. 23 (2), 1199–1210. https://doi.org/10.5194/hess-23-1199-2019.
- Allen, S.T., von Freyberg, J., Weiler, M., Goldsmith, G.R., Kirchner, J.W., 2019b. The seasonal origins of streamwater in Switzerland. Geophys. Res. Lett. 46 (17–18), 10425–10434. https://doi.org/10.1029/2019GL084552.
- Andermann, C., Longuevergne, L., Bonnet, S., Crave, A., Davy, P., Gloaguen, R., 2012. Impact of transient groundwater storage on the discharge of Himalayan rivers. Nat. Geosci. 5 (2), 127–132. https://doi.org/10.1038/ngeo1356.
- Avery, E., Bibby, R., Visser, A., Esser, B., Moran, J., 2018. Quantification of groundwater discharge in a subalpine stream using Radon-222. Water 10 (2), Article 2. https:// doi.org/10.3390/w10020100.
- Azmat, M., Liaqat, U.W., Qamar, M.U., Awan, U.K., 2017. Impacts of changing climate and snow cover on the flow regime of Jhelum River, Western Himalayas. Regional Environ. Change; Dordrecht 17 (3), 813–825. https://doi.org/10.1007/s10113-016-1072-6
- Banks, E.W., Simmons, C.T., Love, A.J., Cranswick, R., Werner, A.D., Bestland, E.A., Wood, M., Wilson, T., 2009. Fractured bedrock and saprolite hydrogeologic controls on groundwater/surface-water interaction: A conceptual model (Australia). Hydrgeol. J. 17 (8), 1969–1989. https://doi.org/10.1007/s10040-009-0490-7.
- Banks, E.W., Simmons, C.T., Love, A.J., Shand, P., 2011. Assessing spatial and temporal connectivity between surface water and groundwater in a regional catchment: Implications for regional scale water quantity and quality. J. Hydrol. 404 (1), 30–49. https://doi.org/10.1016/j.jhydrol.2011.04.017.
- Bavay, M., Lehning, M., Jonas, T., Löwe, H., 2009. Simulations of future snow cover and discharge in Alpine headwater catchments. Hydrol. Process. 23 (1), 95–108. https:// doi.org/10.1002/hyp.7195.
- Beisner, K.R., Gardner, W.P., Hunt, A.G., 2018. Geochemical characterization and modeling of regional groundwater contributing to the Verde River, Arizona between Mormon Pocket and the USGS Clarkdale gage. J. Hydrol. 564, 99–114. https://doi. org/10.1016/i.ihvdrol.2018.06.078.
- Blume, T., van Meerveld, H.J., 2015. From hillslope to stream: Methods to investigate subsurface connectivity. WIREs Water 2 (3), 177–198. https://doi.org/10.1002/ wat2.1071.
- Boano, F., Harvey, J.W., Marion, A., Packman, A.I., Revelli, R., Ridolfi, L., Wörman, A., 2014. Hyporheic flow and transport processes: Mechanisms, models, and biogeochemical implications. Rev. Geophys. 52 (4), 603–679. https://doi.org/10.1002/2012RG000417.
- Bourke, S.A., Cook, P.G., Shanafield, M., Dogramaci, S., Clark, J.F., 2014. Characterisation of hyporheic exchange in a losing stream using radon-222. J. Hydrol. 519, 94–105. https://doi.org/10.1016/j.jhydrol.2014.06.057.
- Bozdogan, H., 1987. Model selection and Akaike's Information Criterion (AIC): The general theory and its analytical extensions. Psychometrika 52 (3), 345–370. https://doi.org/10.1007/BF02294361.
- Brooks, P.D., Gelderloos, A., Wolf, M.A., Jamison, L.R., Strong, C., Solomon, D.K., Bowen, G.J., Burian, S., Tai, X., Arens, S., Briefer, L., Kirkham, T., Stewart, J., 2021. Groundwater-mediated memory of past climate controls water yield in snowmelt-dominated catchments. Water Resour. Res. 57 (10) https://doi.org/10.1029/ 2021WR030605.
- Bush, S.A., Birch, A.L., Warix, S.R., Sullivan, P.L., Gooseff, M.N., McKnight, D.M., Barnard, H.R., 2023. Dominant source areas shift seasonally from longitudinal to lateral contributions in a montane headwater stream. J. Hydrol. 617, 129134 https://doi.org/10.1016/j.jhydrol.2023.129134.
- Carroll, R.W.H., Bearup, L.A., Brown, W., Dong, W., Bill, M., Willlams, K.H., 2018. Factors controlling seasonal groundwater and solute flux from snow-dominated basins. Hydrol. Process. 32 (14), 2187–2202. https://doi.org/10.1002/hyp.13151.
- Carroll, R.W.H., Gochis, D., Williams, K.H., 2020. Efficiency of the summer monsoon in generating streamflow within a snow-dominated headwater basin of the Colorado River. Geophys. Res. Lett. 47 (23) https://doi.org/10.1029/2020GL090856.
- Cartwright, I., Hofmann, H., 2016. Using radon to understand parafluvial flows and the changing locations of groundwater inflows in the Avon River, southeast Australia. Hydrol. Earth Syst. Sci. 20 (9), 3581–3600. https://doi.org/10.5194/hess-20-3581-2016.
- Cook, P.G., Herczeg, A.L. (2000). Environmental tracers in subsurface hydrology. Springer Science + Business Media, LLC.
- Clow, D.W., 2010. Changes in the Timing of Snowmelt and Streamflow in Colorado: A Response to Recent Warming. J. Climate 23, 2293–2306. https://doi.org/10.1175/ 2009JCIJ2951.1.
- Cook, P.G., Lamontagne, S., Berhane, D., Clark, J.F., 2006. Quantifying groundwater discharge to Cockburn River, southeastern Australia, using dissolved gas tracers 222Rn and SF6. Water Resour. Res. 42 (10) https://doi.org/10.1029/ 2006WR004921.

- Cook, B.I., Seager, R., 2013. The response of the North American Monsoon to increased greenhouse gas forcing. J. Geophys. Res. Atmos. 118 (4), 1690–1699. https://doi. org/10.1002/jerd.50111
- Covino, T., 2017. Hydrologic connectivity as a framework for understanding biogeochemical flux through watersheds and along fluvial networks. Geomorphology 277, 133–144. https://doi.org/10.1016/j.geomorph.2016.09.030.
- Cowie, R.M., Knowles, J.F., Dailey, K.R., Williams, M.W., Mills, T.J., Molotch, N.P., 2017. Sources of streamflow along a headwater catchment elevational gradient. J. Hydrol. 549, 163–178. https://doi.org/10.1016/j.jhydrol.2017.03.044.
- Dwivedi, R., Meixner, T., McIntosh, J.C., Ferré, P.A.T., Eastoe, C.J., Niu, G.-Y., Minor, R. L., Barron-Gafford, G.A., Chorover, J., 2019. Hydrologic functioning of the deep critical zone and contributions to streamflow in a high-elevation catchment: Testing of multiple conceptual models. Hydrol. Process. 33 (4), 476–494. https://doi.org/10.1002/hyp.13363.
- Ehsani, M.R., Behrangi, A., 2022. A comparison of correction factors for the systematic gauge-measurement errors to improve the global land precipitation estimate. J. Hydrol. 610, 127884 https://doi.org/10.1016/j.jhydrol.2022.127884.
- Ficklin, D.L., Stewart, I.T., Maurer, E.P., 2013. Climate Change Impacts on Streamflow and Subbasin-Scale Hydrology in the Upper Colorado River Basin. PLoS One 8 (8), e71297
- Fischer, B.M.C., Rinderer, M., Schneider, P., Ewen, T., Seibert, J., 2015. Contributing sources to baseflow in pre-alpine headwaters using spatial snapshot sampling. Hydrol. Process. 29 (26), 5321–5336. https://doi.org/10.1002/hyp.10529.
- Flerchinger, G., Deng, Y., Cooley, K. (1993). Groundwater response to snowmelt in a mountainous watershed: Testing of a conceptual model. doi: 10.1016/0022-1694(93) 90146-Z.
- Floriancic, M.G., van Meerveld, I., Smoorenburg, M., Margreth, M., Naef, F., Kirchner, J. W., Molnar, P., 2018. Spatio-temporal variability in contributions to low flows in the high Alpine Poschiavino catchment. Hydrol. Process. 32 (26), 3938–3953. https://doi.org/10.1002/hyp.13302.
- Gardner, W.P., Harrington, G.A., Solomon, D.K., Cook, P.G., 2011. Using terrigenic 4He to identify and quantify regional groundwater discharge to streams. Water Resour. Res. 47 (6) https://doi.org/10.1029/2010WR010276.
- Gaskill, D.L., 1991. Geologic Map of the Gothic Quadrangle. Gunnison County, Colorado. Genereux, D.P., Hemond, H.F., Mulholland, P.J., 1993. Use of radon-222 and calcium as tracers in a three-end-member mixing model for streamflow generation on the West Fork of Walker Branch Watershed. J. Hydrol. 142 (1), 167–211. https://doi.org/10.1016/0022-1694(93)90010-7.
- Gleeson, T., Manning, A.H., Popp, A., Zane, M., Clark, J.F., 2018. The suitability of using dissolved gases to determine groundwater discharge to high gradient streams. J. Hydrol. 557, 561–572. https://doi.org/10.1016/j.jhydrol.2017.12.022.
- Gooseff, M.N., 2010. Defining hyporheic zones Advancing our conceptual and operational definitions of where stream water and groundwater meet. Geogr. Compass 4 (8), 945–955. https://doi.org/10.1111/j.1749-8198.2010.00364.x.
- Gordon, R.P., Lautz, L.K., McKenzie, J.M., Mark, B.G., Chavez, D., Baraer, M., 2015. Sources and pathways of stream generation in tropical proglacial valleys of the Cordillera Blanca, Peru. J. Hydrol. 522, 628–644. https://doi.org/10.1016/j. jhydrol.2015.01.013.
- Guyer, J.E., Wheeler, D., Warren, J.A., 2009. FiPy: Partial differential equations with python. Comput. Sci. Eng. 11 (3), 6–15. https://doi.org/10.1109/MCSE.2009.52.
- Heidbüchel, I., Troch, P.A., Lyon, S.W., 2013. Separating physical and meteorological controls of variable transit times in zero-order catchments. Water Resour. Res. 49 (11), 7644–7657. https://doi.org/10.1002/2012WR013149.
- Herron, N., Wilson, C., 2001. A water balance approach to assessing the hydrologic buffering potential of an alluvial fan. Water Resour. Res. 37 (2), 341–351. https://doi.org/10.1029/2000WR900253.
- Horton, J.D., San Juan, C.A., Stoeser, D.B., 2017. The State Geologic Map Compilation (SGMC) geodatabase of the conterminous United States (ver. 1.1, August 2017): U.S. Geological Survey Data Series 1052, 46. https://doi.org/10.3133/ds1052.
- Hua, D., Hao, X., Zhang, Y., Qin, J., 2020. Uncertainty assessment of potential evapotranspiration in arid areas, as estimated by the Penman-Monteith method. J. Arid. Land 12 (1), 166–180. https://doi.org/10.1007/s40333-020-0093-7.
- Hubbard, S.S., Williams, K.H., Agarwal, D., Banfield, J., Beller, H., Bouskill, N., Brodie, E., Carroll, R., Dafflon, B., Dwivedi, D., Falco, N., Faybishenko, B., Maxwell, R., Nico, P., Steefel, C., Steltzer, H., Tokunaga, T., Tran, P.A., Wainwright, H., Varadharajan, C., 2018. The East River, Colorado, Watershed: A mountainous community testbed for improving predictive understanding of multiscale hydrological-biogeochemical dynamics. Vadose Zone J. 17 (1), 180061 https://doi.org/10.2136/vzj2018.03.0061.
- Jencso, K.G., McGlynn, B.L., Gooseff, M.N., Bencala, K.E., Wondzell, S.M., 2010. Hillslope hydrologic connectivity controls riparian groundwater turnover: Implications of catchment structure for riparian buffering and stream water sources. Water Resour. Res. 46 (10) https://doi.org/10.1029/2009WR008818.
- Johnson, K., Harpold, A., Carroll, R.W.H., Barnard, H., Raleigh, M.S., Segura, C., Li, L., Williams, K.H., Dong, W., Sullivan, P.L., 2023. Leveraging groundwater dynamics to improve predictions of summer low-flow discharges. Water Resour. Res. 59 (8) https://doi.org/10.1029/2023WR035126.
- Julander, R.P., Clayton, J.A., 2018. Determining the proportion of streamflow that is generated by cold season processes versus summer rainfall in Utah, USA. J. Hydrol.: Reg. Stud. 17, 36–46. https://doi.org/10.1016/j.ejrh.2018.04.005.
- Kapnick, S., Hall, A., 2012. Causes of recent changes in western North American snowpack. Clim. Dyn. 38 (9–10), 1885–1900. https://doi.org/10.1007/s00382-011-1089-y.
- Käser, D., Hunkeler, D., 2016. Contribution of alluvial groundwater to the outflow of mountainous catchments. Water Resour. Res. 52 (2), 680–697. https://doi.org/ 10.1002/2014WR016730.

- Kingston, D.G., Todd, M.C., Taylor, R.G., Thompson, J.R., Arnell, N.W., 2009. Uncertainty in the estimation of potential evapotranspiration under climate change. Geophys. Res. Lett. 36 (20) https://doi.org/10.1029/2009GL040267.
- Kirchner, J.W., 2009. Catchments as simple dynamical systems: Catchment characterization, rainfall-runoff modeling, and doing hydrology backward. Water Resour. Res. 45 (2) https://doi.org/10.1029/2008WR006912.
- Larson, L.W., Peck, E.L., 1974. Accuracy of precipitation measurements for hydrologic modeling. Water Resour. Res. 10 (4), 857–863. https://doi.org/10.1029/ WR010i004p00857.
- Liao, F., Cardenas, M.B., Ferencz, S.B., Chen, X., Wang, G., 2021. Tracing bank storage and hyporheic exchange dynamics using 222Rn: Virtual and field tests and comparison with other tracers. Water Resour. Res. 57 (5) https://doi.org/10.1029/ 2020WR028960.
- Liu, F., Williams, M.W., Caine, N., 2004. Source waters and flow paths in an alpine catchment, Colorado Front Range, United States. Water Resour. Res. 40 (9) https:// doi.org/10.1029/2004WR003076.
- Ludwig, K.R. 2012. User's manual for Isoplot version 3.75–4.15: A geochronological toolkit for Microsoft Excel: Berkeley Geochronological Center Special Publication 5.
- Manning, A.H., Verplanck, P.L., Mast, M.A., Wanty, R.B., 2008, Hydrogeochemical investigation of the Standard Mine vicinity, upper Elk Creek Basin, Colorado: U.S. Geological Survey Scientific Investigations Report 2007–5265, 131 p.
- Mastrotheodoros, T., Pappas, C., Molnar, P., Burlando, P., Manoli, G., Parajka, J., Rigon, R., Szeles, B., Bottazzi, M., Hadjidoukas, P., Fatichi, S., 2020. More green and less blue water in the Alps during warmer summers. Nat. Clim. Change 10 (2), Article 2. https://doi.org/10.1038/s41558-019-0676-5.
- Maurice, L., Rawlins, B.G., Farr, G., Bell, R., Gooddy, D.C., 2017. The influence of flow and bed slope on gas transfer in steep streams and their implications for evasion of CO₂. J. Geophys. Res. Biogeo. 122 (11), 2862–2875. https://doi.org/10.1002/ 2017.IG004045.
- Mayer, T.D., Naman, S.W., 2011. Streamflow response to climate as influenced by geology and elevation1. JAWRA J. Am. Water Resour. Assoc. 47 (4), 724–738. https://doi.org/10.1111/j.1752-1688.2011.00537.x.
- McClymont, A.F., Hayashi, M., Bentley, L.R., Liard, J., 2012. Locating and characterising groundwater storage areas within an alpine watershed using time-lapse gravity, GPR and seismic refraction methods. Hydrol. Process. 26 (12), 1792–1804. https://doi. org/10.1002/hyp.9316.
- McDonnell, J.J., 1990. A rationale for old water discharge through macropores in a steep, humid catchment. Water Resour. Res. 26 (11), 2821–2832. https://doi.org/ 10.1029/WR026i011p02821.
- McIntosh, J.C., Schaumberg, C., Perdrial, J., Harpold, A., Vázquez-Ortega, A., Rasmussen, C., Vinson, D., Zapata-Rios, X., Brooks, P.D., Meixner, T., Pelletier, J., Derry, L., Chorover, J., 2017. Geochemical evolution of the Critical Zone across variable time scales informs concentration-discharge relationships: Jemez River Basin Critical Zone Observatory. Water Resour. Res. 53 (5), 4169–4196. https://doi. org/10.1002/2016WR019712.
- Milly, P.C.D., Dunne, K.A., 2020. Colorado River flow dwindles as warming-driven loss of reflective snow energizes evaporation. Science (New York, N.Y.) 367 (6483), 1252–1255. https://doi.org/10.1126/science.aay9187.
- Mote, P.W., Li, S., Lettenmaier, D.P., Xiao, M., Engel, R., 2018. Dramatic declines in snowpack in the western US. NPJ Clim. Atmos. Sci. 1 (1), 2. https://doi.org/ 10.1038/s41612-018-0012-1.
- Mullinger, N.J., Pates, J.M., Binley, A.M., Crook, N.P., 2009. Controls on the spatial and temporal variability of 222Rn in riparian groundwater in a lowland Chalk catchment. J. Hydrol. 376 (1), 58–69. https://doi.org/10.1016/j. ibydrol.2009.07.015
- Oxtobee, J.P.A., Novakowski, K.S., 2003. Ground water/surface water interaction in a fractured rock aquifer. Groundwater 41 (5), 667–681. https://doi.org/10.1111/ii.1745-6584.2003.th02405.x
- Peterson, R.N., Santos, I.R., Burnett, W.C., 2010. Evaluating groundwater discharge to tidal rivers based on a Rn-222 time-series approach. Estuar. Coast. Shelf Sci. 86 (2), 165–178. https://doi.org/10.1016/j.ecss.2009.10.022.

 Rademacher, L.K., Clark, J.F., Clow, D.W., Hudson, G.B., 2005. Old groundwater
- Rademacher, L.K., Clark, J.F., Clow, D.W., Hudson, G.B., 2005. Old groundwater influence on stream hydrochemistry and catchment response times in a small Sierra Nevada catchment: Sagehen Creek, California. Water Resour. Res. 41 (2) https://doi. org/10.1029/2003WR002805.
- Raymond, P.A., Zappa, C.J., Butman, D., Bott, T.L., Potter, J., Mulholland, P., Laursen, A. E., McDowell, W.H., Newbold, D., 2012. Scaling the gas transfer velocity and hydraulic geometry in streams and small rivers. Limnol. Oceanogr. Fluids Environ. 2 (1), 41–53. https://doi.org/10.1215/21573689-1597669.
- Ryken, A.C., Gochis, D., Maxwell, R.M., 2022. Unravelling groundwater contributions to evapotranspiration and constraining water fluxes in a high-elevation catchment. Hydrol. Process. 36 (1), e14449. https://doi.org/10.1002/hyp.14449.
- Safeeq, M., Grant, G.E., Lewis, S.L., Tague, C.L., 2013. Coupling snowpack and groundwater dynamics to interpret historical streamflow trends in the western United States: COUPLING SNOWPACK AND GROUNDWATER DYNAMICS TO INTERPRET STREAMFLOW. Hydrol. Process. 27 (5), 655–668. https://doi.org/ 10.1002/hyp.9628.
- Salve, R., Rempe, D.M., Dietrich, W.E., 2012. Rain, rock moisture dynamics, and the rapid response of perched groundwater in weathered, fractured argillite underlying a steep hillslope. Water Resour. Res. 48 (11) https://doi.org/10.1029/ 2013WB013583
- Sayama, T., McDonnell, J.J., Dhakal, A., Sullivan, K., 2011. How much water can a watershed store? Hydrol. Process. 25 (25), 3899–3908. https://doi.org/10.1002/ hvp.8388
- Schmidt, A., Gibson, J.J., Santos, I.R., Schubert, M., Tattrie, K., Weiss, H., 2010. The contribution of groundwater discharge to the overall water budget of two typical

- Boreal lakes in Alberta/Canada estimated from a radon mass balance. Hydrol. Earth Syst. Sci. 14 (1), 79–89. https://doi.org/10.5194/hess-14-79-2010.
- Schneider, J.M., Rickenmann, D., Turowski, J.M., Kirchner, J.W., 2015. Self-adjustment of stream bed roughness and flow velocity in a steep mountain channel. Water Resour. Res. 51 (10), 7838–7859. https://doi.org/10.1002/2015WR016934.
- Schubert, M., Siebert, C., Knoeller, K., Roediger, T., Schmidt, A., Gilfedder, B., 2020. Investigating groundwater discharge into a major river under low flow conditions based on a radon mass balance supported by tritium data. Water 12 (10), 2838. https://doi.org/10.3390/w12102838.
- Segura, C., Noone, D., Warren, D., Jones, J.A., Tenny, J., Ganio, L.M., 2019. Climate, landforms, and geology affect baseflow sources in a mountain catchment. Water Resour. Res. 55 (7), 5238–5254. https://doi.org/10.1029/2018WR023551.
- Sheppard, P.R., Comrie, A.C., Packin, G.D., Angersbach, K., Hughes, M.K., 2002. The climate of the US Southwest. Clim. Res. 21 (3), 219–238. https://doi.org/10.3354/ cr021219
- Singh, N.K., Emanuel, R.E., McGlynn, B.L., 2016. Variability in isotopic composition of base flow in two headwater streams of the southern Appalachians. Water Resour. Res. 52 (6), 4264–4279. https://doi.org/10.1002/2015WR018463.
- Smerdon, B.D., Gardner, W.P., 2022. Characterizing groundwater flow paths in an undeveloped region through synoptic river sampling for environmental tracers. Hydrol. Process. 36 (1), e14464.
- Smerdon, B.D., Payton Gardner, W., Harrington, G.A., Tickell, S.J., 2012. Identifying the contribution of regional groundwater to the baseflow of a tropical river (Daly River, Australia). J. Hydrol. 464–465, 107–115. https://doi.org/10.1016/j. jhydrol.2012.06.058.
- Somers, L.D., McKenzie, J.M., 2020. A review of groundwater in high mountain environments. WIREs Water 7 (6), e1475.
- Somers, L.D., McKenzie, J.M., 2020. A review of groundwater in high mountain environments. WIREs Water 7 (6), e1475.
- Somers, L.D., McKenzie, J.M., Mark, B.G., Lagos, P., Ng, G.-H.-C., Wickert, A.D., Yarleque, C., Baraër, M., Silva, Y., 2019. Groundwater Buffers decreasing glacier melt in an andean watershed—But not forever. Geophys. Res. Lett. 46 (22), 13016–13026. https://doi.org/10.1029/2019GL084730.
- Spence, C., 2007. On the relation between dynamic storage and runoff: A discussion on thresholds, efficiency, and function. Water Resour. Res. 43 (12) https://doi.org/ 10.1029/2006WR005645
- Spencer, S.A., Anderson, A.E., Silins, U., Collins, A.L., 2021. Hillslope and groundwater contributions to streamflow in a Rocky Mountain watershed underlain by glacial till and fractured sedimentary bedrock. Hydrol. Earth Syst. Sci. 25 (1), 237–255. https://doi.org/10.5194/hess-25-237-2021.
- Sprenger, M., Carroll, R.W.H., Dennedy-Frank, J., Siirila-Woodburn, E.R., Newcomer, M. E., Brown, W., Newman, A., Beutler, C., Bill, M., Hubbard, S.S., Williams, K.H., 2022. Variability of snow and rainfall partitioning into evapotranspiration and summer

- runoff across nine mountainous catchments. Geophys. Res. Lett. 49 (13) https://doi.org/10.1029/2022GL099324.
- Stewart, I.T., Cayan, D.R., Dettinger, M.D., 2005. Changes toward earlier streamflow timing across Western North America. J. Clim. 18 (8), 1136–1155. https://doi.org/ 10.1175/JCLJ3321.1.
- Ulseth, A.J., Hall, R.O., Boix Canadell, M., Madinger, H.L., Niayifar, A., Battin, T.J., 2019. Distinct air–water gas exchange regimes in low- and high-energy streams. Nat. Geosci. 12 (4), Article 4. https://doi.org/10.1038/s41561-019-0324-8.
- Verplanck, P.L., Manning, A.H., Graves, J.T., McCleskey, R.B., Todorov, Todor, Lamothe, P.J., 2010, Geochemistry of Standard Mine waters, Gunnison County, Colorado, July 2009: U.S. Geological Survey Open-File Report 2009–1292, 21 p.
- Viviroli, D., Dürr, H.H., Messerli, B., Meybeck, M., Weingartner, R., 2007. Mountains of the world, water towers for humanity: Typology, mapping, and global significance. Water Resour. Res. 43 (7) https://doi.org/10.1029/2006WR005653.
- Viviroli, D., Kummu, M., Meybeck, M., Kallio, M., Wada, Y., 2020. Increasing dependence of lowland populations on mountain water resources. Nat. Sustainability 3 (11), Article 11. https://doi.org/10.1038/s41893-020-0559-9.
- Wanninkhof, R., Mulholland, P.J., Elwood, J.W., 1990. Gas exchange rates for a first-order stream determined with deliberate and natural tracers. Water Resour. Res. 26 (7), 1621–1630. https://doi.org/10.1029/WR026i007p01621.
- Webb, J.R., Santos, I.R., Robson, B., Macdonald, B., Jeffrey, L., Maher, D.T., 2017. Constraining the annual groundwater contribution to the water balance of an agricultural floodplain using radon: The importance of floods. Water Resour. Res. 53 (1), 544–562. https://doi.org/10.1002/2016WR019735.
- Westerhoff, R.S., 2015. Using uncertainty of Penman and Penman-Monteith methods in combined satellite and ground-based evapotranspiration estimates. Remote Sens. Environ. 169, 102–112. https://doi.org/10.1016/j.rse.2015.07.021.
- Wittenberg, H., Aksoy, H., Miegel, K., 2019. Fast response of groundwater to heavy rainfall. J. Hydrol. 571, 837–842. https://doi.org/10.1016/j.jhydrol.2019.02.037.
- Xiao, X., Zhang, X., Wu, H., Zhang, C., Han, L., 2022. Stable isotopes of surface water and groundwater in a typical subtropical basin in south-central China: Insights into the young water fraction and its seasonal origin. Hydrol. Process. 36 (4), e14574
- Zelazny, M., Astel, A., Wolanin, A., Małek, S., 2011a. Spatiotemporal dynamics of spring and stream water chemistry in a high-mountain area. Environ. Pollut. 159 (5), 1048–1057. https://doi.org/10.1016/j.envpol.2010.11.021.
- Żelazny, M., Astel, A., Wolanin, A., Małek, S., 2011b. Spatiotemporal dynamics of spring and stream water chemistry in a high-mountain area. Environ. Pollut. 159 (5), 1048–1057. https://doi.org/10.1016/j.envpol.2010.11.021.
- Zhi, W., Li, L., Dong, W., Brown, W., Kaye, J., Steefel, C., Williams, K.H., 2019. Distinct source water chemistry shapes contrasting concentration-discharge patterns. Water Resour. Res. 55 (5), 4233–4251. https://doi.org/10.1029/2018WR024257.
- Zuecco, G., Penna, D., Borga, M., 2018. Runoff generation in mountain catchments: Long-term hydrological monitoring in the Rio Vauz Catchment, Italy. Cuadernos De Investigación Geográfica 44 (2), Article 2. https://doi.org/10.18172/cig.3327.